# Process-parameter-dependent optical and structural properties of $ZrO_2MgO$ mixed-composite films evaporated from the solid solution

N. K. Sahoo and A. P. Shapiro

The process-parameter-dependent optical and structural properties of $ZrO_2MgO$ mixed-composite material have been investigated. Optical properties were derived from spectrophotometric measurements. By use of atomic force microscopy, x-ray diffraction analysis, and energy-dispersive x-ray (EDX) analysis, the surface morphology, grain size distributions, crystallographic phases, and process-dependent material composition of films have been investigated. EDX analysis made evident the correlation between the oxygen enrichment in the films prepared at a high level of oxygen pressure and the very low refractive index. Since oxygen pressure can be dynamically varied during a deposition process, coatings constructed of suitable mixed-composite thin films can benefit from continuous modulation of the index of refraction. A step modulation approach is used to develop various multilayer-equivalent thin-film devices.

*OCIS codes:* 160.4670, 240.0310, 310.1620, 310.6860, 310.3840, 310.1860.

## 1. Introduction

In spite of all the modern technological advancements in coating processes and controls, the problem of identifying optimum optical materials for developing precision thin-film devices still remains. The use of conventional multilayer thin-film structures fails to meet the changeable, yet demanding, requirements of high-power laser, cryogenic, and space-based technologies. Especially in the case in which high-intensity electromagnetic radiation is present, the discrete refractive indices ($H$, $L$, $M$, etc.) result in multitransition in the electric-field amplitude within a multilayer stack. Alternatively, the most promising approach is to use continuously varying refractive-index and composition profiles, thus avoiding standing-wave electric-field distributions associated with discrete multilayer boundaries. The important inherent advantages of such configurations over multilayer filter stacks is the absence of discrete interface layers, often the source of light-scattering defects, and the increased design versatility due to the availability of a full range of refractive indices as opposed to limited discrete values.[1,2]

In this study, we have studied the process-dependent optical and structural properties of mixed-composite $ZrO_2MgO$ films deposited from the solid solution, and we have successfully achieved tunability of the refractive index. During the course of this investigation, we found an interesting dominant effect of oxygen pressure on the film's optical properties. In the higher range of oxygen pressure, we observed a dramatic lowering of refractive indices. Various kinds of optical inhomogeneities were also observed when different process parameters were systematically altered. Optical properties and constants have been derived from the transmittance and the reflectance spectra of the films recorded during and after the process. Through atomic force microscopy (AFM), the surface structures and power spectral densities (PSD's) of critical films have been investigated. Combinations of other characterization techniques, such as x-ray diffraction analysis and energy-dispersive x-ray (EDX) via scanning electron microscopy (SEM), provided much valuable information about the process-dependent microstructure of the films. Note that the refractive index of the

The authors are with NASA Marshall Space Flight Center, Mail Code: EB52, Huntsville, Alabama 35812. The permanent address for N. K. Sahoo is Spectroscopy Division, BARC, Bombay-40085, India.

Received 7 July 1997; revised manuscript received 22 September 1997.

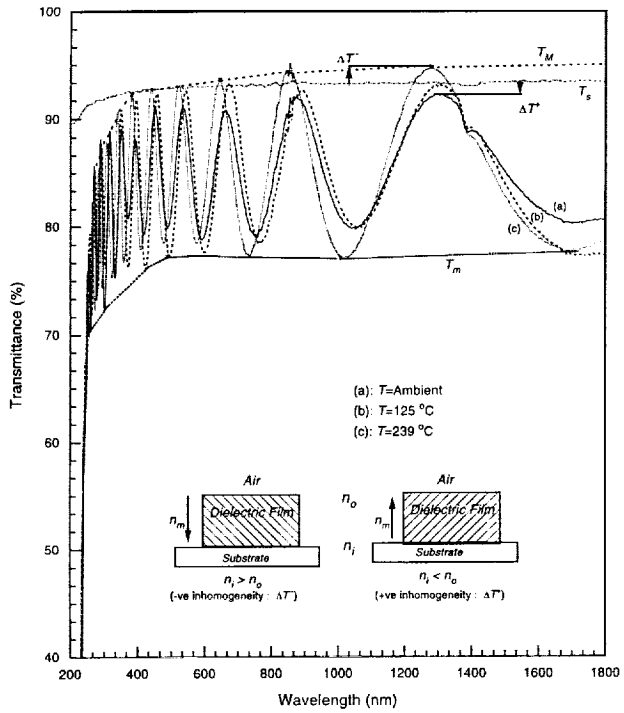


Fig. 1. Transmittance characteristics of three experimental films deposited under different substrate temperatures, but with the same deposition rate and oxygen pressure. $T_s$ is the substrate transmittance, $T_M$ and $T_m$ are the envelopes for the maxima and the minima. $\Delta T'$ and $\Delta T''$ are the decrease and the increase of the transmittance value at half-wave points corresponding to positive and negative inhomogeneity.

solid solution varies from a quite low value to an appreciable higher value as a function of oxygen pressure in certain deposition conditions. Oxygen pressure can be dynamically varied during the deposition process, which allows one to generate coatings with continuously variable refractive indices.

Many thin-film researchers have concluded that substrate temperature is one of the most dominant parameters for controlling the microstructure and the optical constants during the growth of oxide dielectric films.[3–5] Changing the temperature of the substrate, however, is a very slow process. Hence it is highly inconvenient to use this parameter for modulating the deposition process. However, in our experiment, it is observed that by varying substrate temperature, it is possible to change the nature and the extent of the inhomogeneity from positive to negative. Films deposited in certain deposition conditions showed an initial homogeneous structure within the first few quarter-wave turning points (critical thickness) followed by a transition to inhomogeneity. An experimental film of this type, deposited at optimized temperature and at a high rate of evaporation, has been described in the sections below.

## 2. Earlier Research on Coevaporated Mixed Films

Tunability of the refractive index of mixed-material optical thin films has created significant interest in the area of thin-film coatings. It is possible to develop more complex multilayer thin-film devices by using a variable refractive-index material in the design. For example, through the controlled variation of refractive index with respect to layer thickness, optical coatings such as rugate filters, wide-band antireflection coatings, nonpolarizing beam splitters, and minus filters can be developed to the desired specifications in the best possible manner.[6,7] Obtaining such optical properties experimentally, however, is quite intricate. The theoretical aspect of development of optical coatings with continuously varying refractive index has been investigated by Jacobsson[8,9] in great detail. Although coevaporation has been tried by many thin-film researchers to achieve the tunability, the methodology is still not well developed. This is due to the complexity in the process control caused by the large number of deposition parameters that are required when independent sources are utilized. For example, there have been reports on the double electron-beam coevaporation of mixed films of $ZrO_2$–$SiO_2$,[10] $TiO_2$–$SiO_2$,[3] $ZrO_2$–$Y_2O_3$,[11,12] $ZrO_2$–$Al_2O_3$,[13] $HfO_2$–$MgF_2$,[14] $ZrO_2$–$Ta_2O_5$,[4] $Ta_2O_5$–$TiO_2$,[4] $In_2O_3$–$ZrO_2$,[15] $ZrO_2$–$ZnO$,[5] and $ZrO_2$–$MgO$.[16–18] In this approach it is possible to obtain a refractive index of the mixed film at any desired value between lower- and upper-index component values by suitably controlling the rate of evaporation of individual sources.[3] This approach is quite involved, as the coating system has to be equipped with at least two different sources with necessary feedback controllers for measuring and controlling the dynamics of the deposition process.

Most recently, the potential of tuning optical and structural properties of solid solution composite materials has created a substantial interest in the development of advanced multilayer structures. The formation of solid solutions in semiconductors and dielectrics is important, since it very often leads to a material with quite new optical and physical proper-

**Table 1. Sellmier Coefficients for the Films Deposited at the Same Rate of Deposition (1 Å/s), Without Any Additional Oxygen, at Various Substrate Temperatures**

| Sub. Temp in °C | Coefficient '$A$' | Coefficient '$B_1$' | Coefficient '$B_2$' × $10^4$ | Coefficient '$C_1$' | Coefficient '$C_2$' × $10^8$ |
|---|---|---|---|---|---|
| Ambient | 1.0801 | 2.4601 | 2.135 | 18.633 | 5.76 |
| 125 | 2.3476 | 1.3644 | 3.0728 | 32.7578 | 5.76 |
| 167 | 2.1834 | 1.7316 | 2.8032 | $2.707 \times 10^{-8}$ | 5.76 |
| 239 | 2.0743 | 1.7372 | 2.7796 | $1.3733 \times 10^{-7}$ | 5.76 |

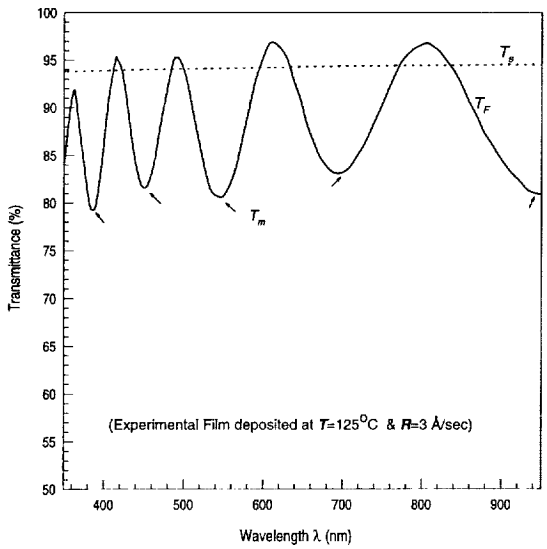


Fig. 2. Transmittance characteristics of a film deposited at a substrate temperature 125 °C, at 3 Å/s and without any additional oxygen. Peak minima ($T_m$'s) shows modulative behavior rather than dispersive for this film.

ties.[19] Recently, the optical structural properties of solid solutions of $ZnSe_xTe_{1-x}$ have been investigated by El-Nahass *et al.*,[20] with the goal of developing photoelectronic devices.[20] It has been established that some of the refractory oxides and rare earths, e.g., $ZrO_2$, $Sc_2O_3$, MgO, $In_2O_3$, $Al_2O_3$, $Y_2O_3$, and CaO, exhibit extended solid solubility among themselves. These mixed-material solid solutions have phase-transformation temperatures and a whole range of new optical, physical and structural properties that are substantially different from those of the individual pure materials.[21] Formation of a solid solution of this sort, however, is possible only among specific crystallographic phases of the oxides. These solid solutions in composite materials are very important for optical-coating applications because of their potential for having tunable properties by means of process modulation.

### 3. Earlier Research on the $ZrO_2$MgO System

Historically, the $ZrO_2$MgO binary system has drawn the attention of so many investigators because of its potential use in structural and corrosion-resistive applications. Magnesia partially stabilized $ZrO_2$ is the toughest monolithic ceramic now known.[22] Although some optical-coating studies have already been reported on for coevaporated $ZrO_2$ + MgO mixed films,[16–19] not much research has been done on its solid solution. Various studies have already been carried out on the equilibrium phase relations in the binary $ZrO_2$ + MgO system.[23–25] Several investigations have reported metastable tetragonal or cubic zirconia following the decomposition of unstabilized and stabilized zirconium-based precursors at temperatures well below that which the stable modifications are known to exist. Ruff and Ebert[26] reported that the two oxides $ZrO_2$ and MgO combined to form a

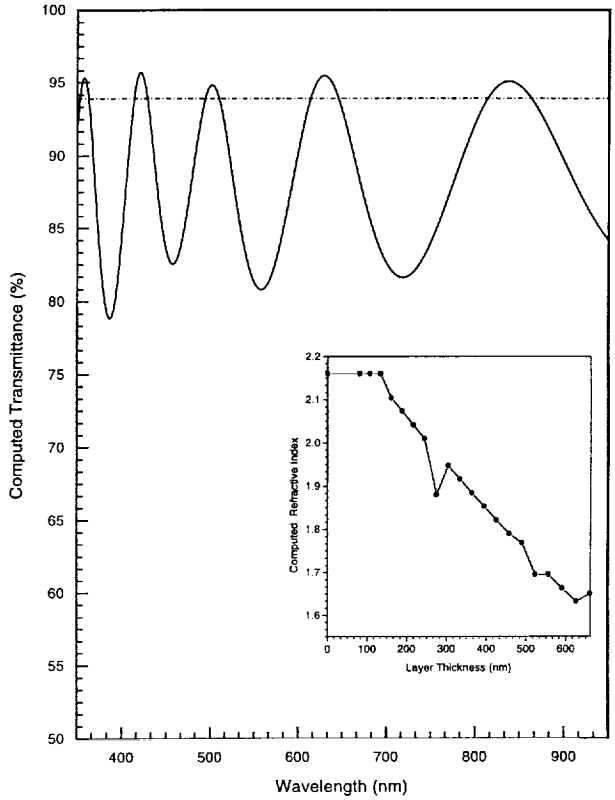


Fig. 3. Modeling of a nonlinear inhomogeneity showing computed transmittance characteristics and computed refractive index versus physical thickness of the layer (inset plot). The film is assumed to be nondispersive and nonabsorbing for simplicity during computation.

cubic phase above 1460 °C. They considered the cubic phase to be a compound having the formula $Mg_2Zr_3O_8$; however, it was later established that $ZrO_2$ and MgO form a limited series of solid solutions rather than a compound. It has also been observed that the probability of MgO forming a solid solution with monoclinic $ZrO_2$ is very limited.[24] During our investigations, we discovered the traces of monoclinic phase in the films deposited in certain ambient conditions.

The microstructural development during the aging of supersaturated solid solutions of cubic $ZrO_2$ stabilized with MgO has been studied by Porter and Heuer[19] using transmission electron microscopy. They observed a very interesting stress-induced transformation leading to a high-fracture toughness during the annealing experiments. The formation of a defect phase $Mg_2Zr_5O_{12}$ (δ) within the cubic matrix at a temperature of 1250 °C has been reported by investigators.[27] With respect to optical-coating applications, however, it is observed that the cubic phase of $ZrO_2$ yields the most favorable optical properties.[28] Studies of MgO-stabilized zirconia optical coatings prepared by double-electron-beam gun evaporation on nickel substrates by Tcheliebou *et al.*[16] have shown an interesting result: They obtained a refractive-index maximum from the samples contain-

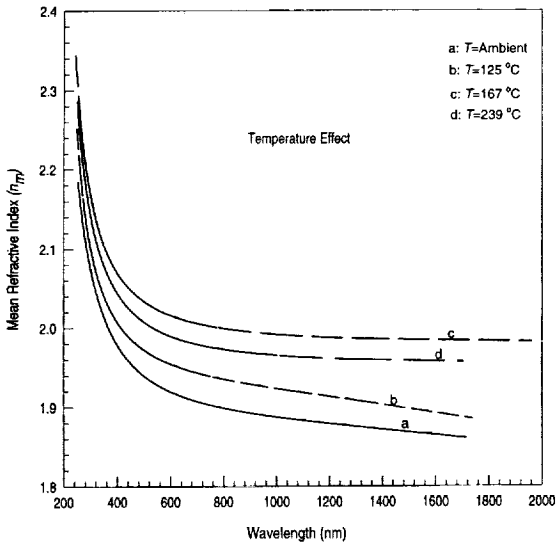


Fig. 4. Refractive indices of films deposited under different substrate temperatures but at the same rate (1 Å/s) and oxygen pressure (base value).

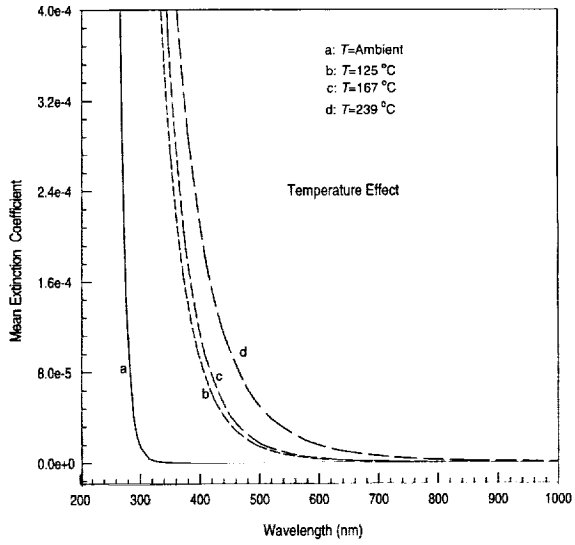


Fig. 5. Extinction coefficients of films deposited under different substrate temperatures but at the same rate (1 Å/s) and oxygen pressure (base value).

ing 15% (molar) MgO in the alloy. At molar percentages of MgO greater than 20%, a monotonic decrease of index and packing density was noted. Similar composition-dependent optical properties were observed in our investigation during optimization of the process parameters for our samples.

## 4. Experimental Details

We deposited mixed-composite films on 25-mm-diameter, 3–5-mm-thick, optically polished quartz and BK7 substrates by evaporating optical-grade $ZrO_2MgO$ solid solution typically 99.7% pure (M/s CERAC Inc., supplied). The deposition chamber used throughout this investigation was a Balzers BAK-760 fully automatic box coater, cryopumped to a base pressure of $8 \times 10^{-7}$ mbar. The material was evaporated from a Temescal CV-8 four-pocket electron-beam source. During the deposition, we controlled the beam position and the scanning manually for the best utilization of the surface of the evaporating material. In this chamber, the substrates can be heated as high as 300 °C by a pair of quartz lamps. The temperature can be controlled by a Eurotherm controller with a repeatability of ±1 °C. The substrates can be preheated or postheated to the desired level by the Balzers BPU-420E process controller. Note that it is difficult to measure the temperature of the rotating substrate during the actual process. We found it necessary to determine a scaling factor experimentally to derive the actual temperature of the substrate from the temperature measured by means of a thermocouple located above the heating sources. For this calibration, we mounted a large piece of plate glass (59 cm × 45 cm) on our rotary planetary and placed the thermocouple in contact with this substrate during rotation. We then measured the equilibrium temperatures achieved as a result of different heat-lamp power settings. The same steps were repeated with the thermocouple located at the measuring position near quartz lamps, and a calibration curve was generated between two sets of measurements. The thermocouple for the Eurotherm controller was precalibrated with the freezing and the boiling points of water.

A fully automatic advanced Balzers GSM-420 optical monitor–controller was used to control and monitor the optical thickness of the growing films. It is also possible to use this system as an *in situ* spectrophotometer over the UV to the near-infrared (NIR) spectral range. Hence the spectral characteristics of the deposited film can be recorded both during and after the deposition and also either inside or outside the vacuum. A Balzers QM-420 six-head quartz-crystal controller was used to control either the physical thickness or the rate of evaporation of the films. The oxygen pressure can be very accurately controlled by a Balzers Model RV-420 mass-flow controller.

During this investigation, the transmittance and the reflectance spectra of the films were recorded with a GSM-420 optical controller during and just after the deposition process. The postdeposition transmittance characteristics in air were recorded with a Perkin–Elmer Lamda-19 UV–vis–NIR spectrophotometer. The extent of inhomogeneity during the growth of film was computed from the *in situ* transmittance data. By use of SPECTR analysis software, developed by Sahoo, the films were characterized for their mean refractive index ($n_m$), extinction coefficient ($k_m$), absorption constant ($\alpha_m$), physical thickness ($d$), and inhomogeneity ($\Delta n$). The phase compositions of films deposited in various process conditions were analyzed through x-ray diffraction. The semiquantitative compositions of the films grown in varying deposition conditions were determined by SEM.

## 5. Spectrophotometric Analysis

There have been several reported efforts to extract the optical constants of inhomogeneous thin films from spectrophotometric data.[29–33] It is now very well accepted that there is always some ambiguity involved in the determination of the constants when only postspectrophotometric measurements are taken into account, especially for nonlinear inhomogeneous films. Fortunately, *in situ* transmittance and reflectance data recorded during the growth of such films may be used to provide the vital information necessary for accurate computation of desired constants. In general, transmittance measurements are more accurate than reflectance.[34,35] Borgogno *et al.*[36] have described the limitation of accuracy obtained during the monitoring of inhomogeneous multilayer systems. A novel technique based on transmittance measurements carried out in vacuum has been developed by Bovard *et al.*[30] to derive the dispersive refractive-index profile and extinction coefficient of inhomogeneous thin films. They used a rapid-scanning monochromator system during the deposition process.

In our present studies, we recorded the transmittance signal at a predetermined wavelength during the growth process, and we scanned the film transmittance in vacuum after the deposition from 350 to 975 nm using the of GSM-420 optical monitor system. Both of these data sets were used in combination with spectral characterizations acquired after exposure to room air at ambient humidity to analyze the inhomogeneity and to determine optical constants. The latter transmittance spectra were recorded on a Perkin–Elmer Lamda-19 UV–vis–NIR spectrophotometer. All spectra were then analyzed to locate their interference peaks using Spectra Calc commercial data-analysis software. The spectrophotometric data sets were then processed by the SPECTR analysis software to compute the mean constants,[29] which include refractive index $n_m$, extinction coefficient $k_m$, absorption constant $\alpha_m$, and physical thickness $d$. The degree of inhomogeneity ($\Delta n^{\mp}$, negative or positive) is computed from the expression assuming the columnar growth of the film as follows[29,37,38]:

$$\Delta n^{\mp} = \frac{n_m \Delta T^{\mp}}{4.4(1 - T_s)}, \tag{1}$$

where $n_m$ is the mean value for the refractive index and $\Delta T^{\mp}$ is the difference of film ($T_F$) and substrate transmission ($T_s$) at the peak maxima. Different types of inhomogeneity with positive and negative values of this parameter are shown in Fig. 1. As illustrated in this figure, when the refractive index of the film at substrate interface ($n_i$) is greater than that of air interface ($n_o$), it results in negative inhomogeneity (antireflection effect) and vice versa for the positive case. Unlike negative inhomogeneity, the positive inhomogeneity cannot be uniquely determined from the transmittance measurements alone. In such films, an additional reflection measurement is needed to resolve the ambiguity.

While computing these parameters, the transmittance data and quartz-crystal data were taken into account to compute the thickness of the inhomogeneous samples. Some of the samples were also examined with a Dektac stylus-type profiler. Since the samples showed a wide range of inhomogeneities changing from linear to hyperbolic or exponential etc., it is not possible to compute an actual refractive-index profile in the growth direction from its transmittance measurements. It is always possible, however, to compute the mean refractive index ($n_m$) from the order of the peaks ($o_m$), experimental peak positions ($\lambda_p$), and thickness value ($d$) as follows[30]:

$$d = o_m \frac{\lambda_p}{4.n_m}, \tag{2}$$

where

$$n_m = \frac{1}{d} \int_0^d n(z)\mathrm{d}z. \tag{3}$$

After getting starting values of $d$ and $n_m$, Eqs. (1)–(3) can be used with any constrained fitting technique to get improved values for the parameters. This information on mean constants is sufficient to characterize the films for their process-parameter-dependent properties. The details of this approach have been described elsewhere.[29] We have found that experimental mean refractive index of the films were fit very well by use of the two-pole Sellmeier dispersion formula[39]:

$$n_m^2(\lambda) = A + B_1/(1 - B_2/\lambda^2) + C_1/(1 - C_2/\lambda^2), \tag{4}$$

where $\lambda$ is the wavelength of the incident light and coefficients $A$, $B_1$, $B_2$, $C_1$, and $C_2$ have their meanings as per Ref. 39. The first and second terms represent, respectively, the contribution to refractive indices due to higher-energy and lower-energy bandgaps of electronic absorption, whereas the last term accounts for a decrease in refractive indices because of lattice absorption. Subsequently, these index fits were refined to match the computed transmittance spectra with experimental curve to a reasonably good accuracy. It is also possible to compute mean electronic bandgaps ($E_g$) from the Sellmeier coefficient $B_2$. In the above expression, the coefficient $C_2$ determines the IR transmission cutoff; it is the square of twice the energy associated with the IR transmission cutoff edge. The computed Sellmeier coefficients for samples prepared under various substrate temperatures but at the same rate of deposition and oxygen pressure are given in Table 1.

Like refractive index, the mean extinction coefficient for inhomogeneous films is defined as

$$k_m = \int_0^d k(z)\mathrm{d}z. \tag{5}$$

In the present case, we computed the extinction coefficients in strong and medium absorbing regions

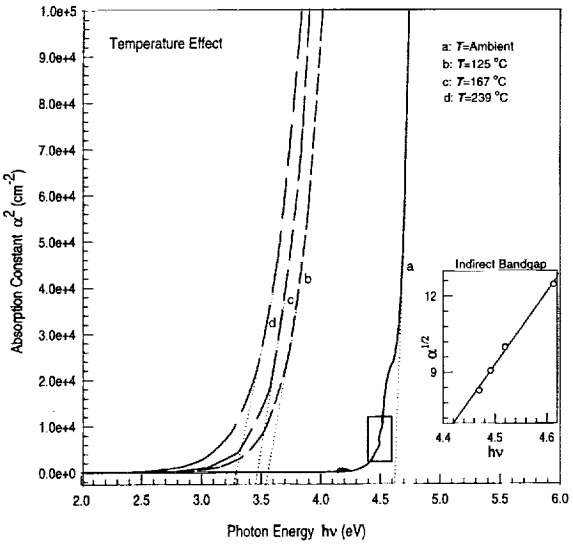


Fig. 6. Bandgaps of films deposited under different substrate temperatures but at the same rate (1 Å/s) and oxygen pressure (base value). Film deposited at ambient temperature shows an additional indirect bandgap (corresponding to α-phase), which is shown in the inset plot.

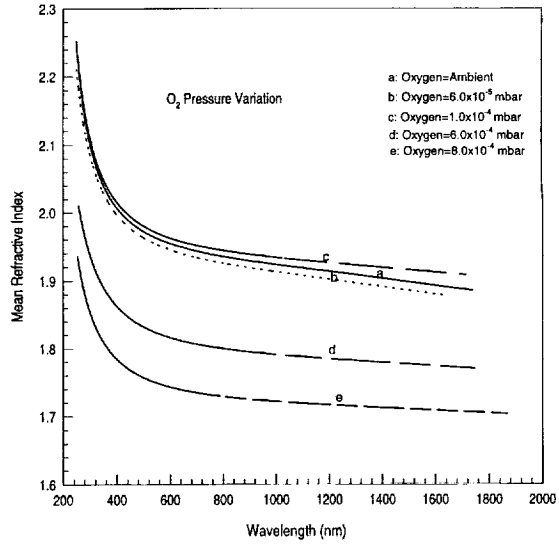


Fig. 7. Refractive indices of films deposited under different oxygen pressures but at the same rate (1 Å/s) and substrate temperature (125 °C).

using $T_\alpha$ and $T_i$, which are the geometric and arithmetic means of $T_M$ and $T_m$, and are defined as[35]

$$T_\alpha = \sqrt{(T_M T_m)}, \tag{6}$$

$$T_i = 2T_M T_m/(T_M + T_m). \tag{7}$$

Variables $T_M$ and $T_m$ are the maxima and the minima transmittance envelopes, respectively, for the interference fringes as shown in Fig. 1. Subsequently, the values were fitted with a suitable equation to compute the constants in the weakly absorbing and transparent region. For our films we found that the extinction coefficients follow a logistic equation very well, which is as follows[29]:

$$k_m(\lambda) = \frac{a}{1 + (\lambda/c)^b}, \tag{8}$$

where $\lambda$ is the wavelength of light and $a$, $b$, and $c$ are the coefficients for fitting.

Besides refractive-index and extinction coefficients, the optical bandgap energy, $E_g$ provides very important information regarding the spectral range over which the desired optical material is useful. Optical absorption edges are not perfectly sharp for dielectric and semiconducting materials. Hence it is necessary to examine more carefully the nature of the absorption process to understand their shapes. Such understandings provide information on the stoichiometry and the phase composition of the material. For a direct bandgap the absorption coefficient for transitions is of the form[40,41]

$$\alpha \sim [\hbar\omega - E_g]^{1/2}, \tag{9}$$

for $\hbar\omega > E_g$,

$$\alpha = 0, \tag{10}$$

for $\hbar\omega < E_g$, and for indirect transitions[42]:

$$\alpha^{1/2} \sim [\hbar\omega - E_g], \tag{11}$$

for $\hbar\omega > E_g$ where $\alpha$ is the absorption constant and $\hbar\omega$ (or $h\nu$) is the photon energy of the incident radiation. In the present case, the process-dependent bandgap values provided very useful information with regard to the phase composition of the films deposited in specific deposition conditions.

## 6. Films with Mixed Inhomogeneity

During our experiments we discovered that in certain process conditions the films showed mixed inhomogeneity, i.e., after certain minimum critical thickness of homogeneous growth, the inhomogeneity began to appear. This phenomenon is observed during in-process optical monitoring. The presence of such a structural condition is also reflected in the postprocess transmittance spectra. In the transmittance spectra, the peak minima show a modulative behavior instead of being dispersive. An experimental $ZrO_2MgO$ film, deposited at a substrate temperature of 125 °C, at a rate of 3 Å/s, and without any additional oxygen, is depicted in Fig. 2.

The computation of optical constants requires much more complex modeling when inhomogenious or mixed growth modes are present. The simulated refractive-index profile and the corresponding calculated transmittance curve for our experimental $ZrO_2MgO$ film are shown in Fig. 3. This spectral characteristic is simulated with a combination of homogeneous and inhomogeneous growth models. We divided the entire thickness of the layer to 20 small discrete sublayers to model the index profile. Dis-

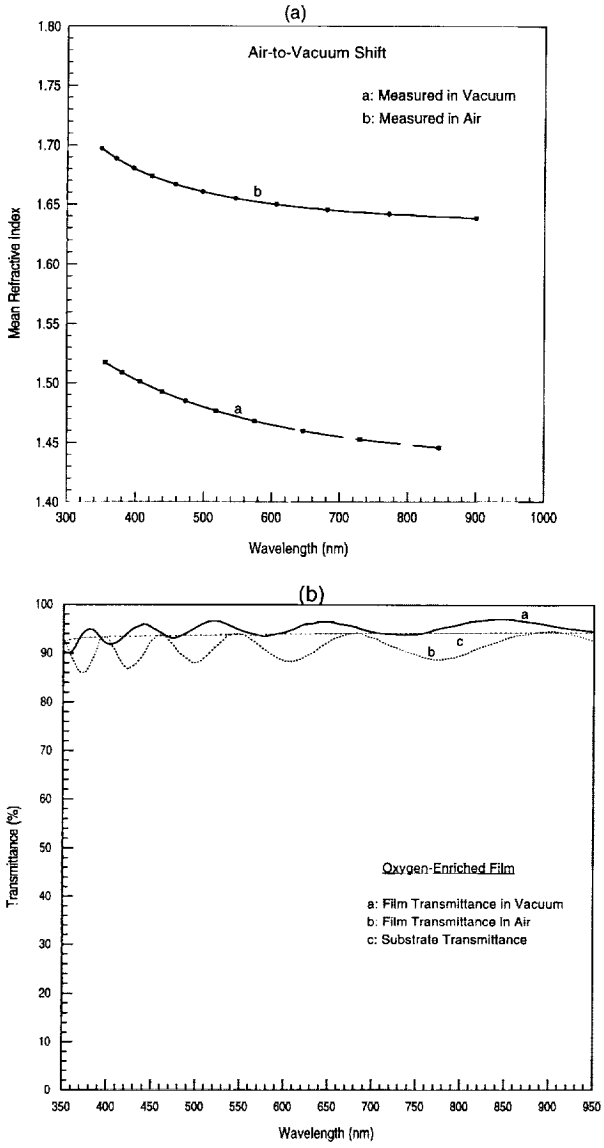


Fig. 8. (a) Air-to-vacuum shift of the refractive index of the film deposited at the higher oxygen pressure of $8 \times 10^{-4}$ mbar. (b) Measured transmittance characteristics of the film deposited at high oxygen pressure ($8 \times 10^{-4}$ mbar) in vacuum and in air.

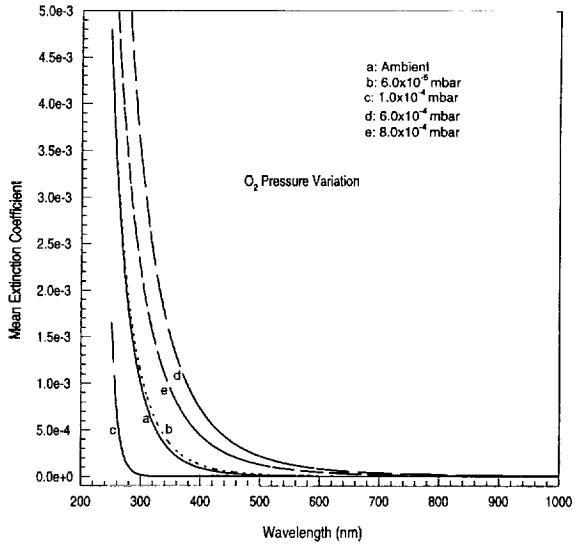


Fig. 9. Extinction coefficients of films deposited under different oxygen pressures but at the same rate (1 Å/s) and substrate temperature (125 °C).

persion in refractive index and extinction coefficients are not taken into account to avoid the complexity in the computation. The simulated refractive-index profile shows a highly nonlinear behavior after a certain critical thickness of homogeneous growth. More detailed analyses on these aspects are being carried out and will be reported very soon. This type of mixed nonlinear inhomogeneity has also been reported by Tikhonravov *et al.*[43] in their study of the refractive-index profile of $ZrO_2$ films with a fast-scanning acousto-optic spectrophotometer.

A growth-dependent stoichiometry, which appears in oxygen-rich polycrystalline MgO films, has been reported by Hebard *et al.*[44] They discovered that a rapid increase of oxygen enrichment beyond a certain critical thickness gives rise to a superstoichiometric structure in sputter-deposited MgO films. They observed an increase of dielectric permittivity by 40% of bulk value in such films. The presence of MgO in the solid solution deposited in specialized conditions in our experiment may be related to the observed inhomogeneity.

### 7. Effect of Substrate Temperature

The substrate temperature was found to have a significant effect on the film optical constants. The films prepared in ambient conditions, i.e., at base vacuum pressure and without quartz lamp heating, exhibited the lowest refractive index as shown in Fig. 4. The maximum index was obtained with a depo-

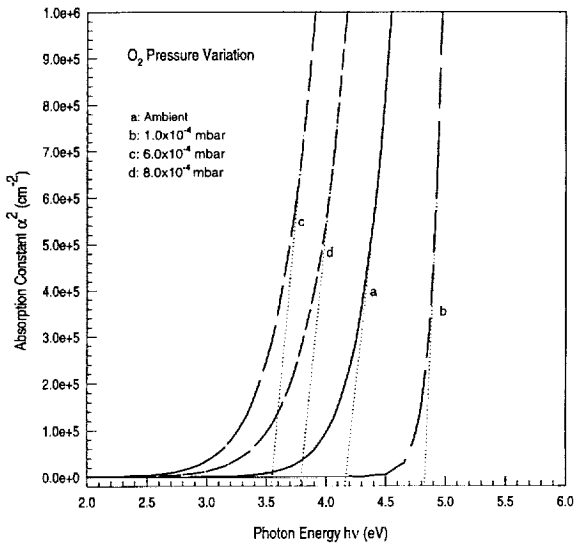


Fig. 10. Bandgaps of films deposited under different oxygen pressures but at the same rate (1 Å/s) and substrate temperature (125 °C).

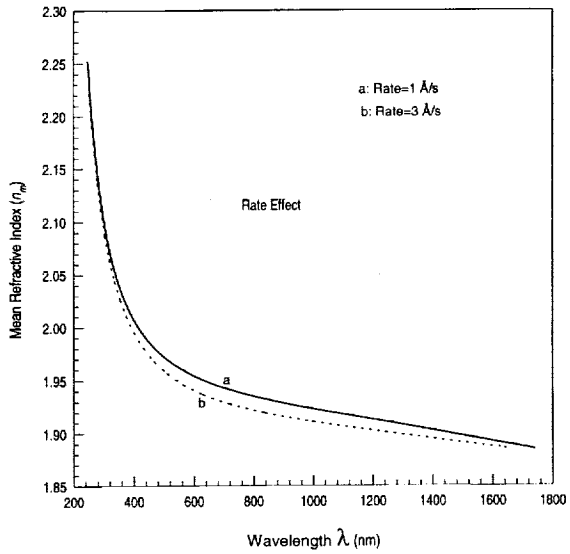


Fig. 11. Refractive indices of films deposited under different rates of evaporation but at the same oxygen pressure (base value) and substrate temperature (125 °C).

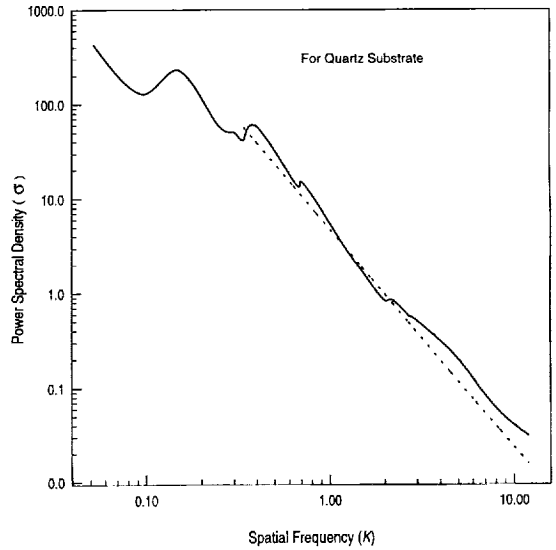


Fig. 13. Plot of PSD of uncoated quartz substrate versus spatial frequency showing a quasi-linear behavior.

sition temperature of 167 °C, but beyond this value, the index variation showed a downward trend. The inhomogeneity in the films also showed a quite significant change from positive to negative as a function of substrate temperature. The films prepared at ambient conditions showed positive inhomogeneity and, at our highest deposition temperature of 239 °C, they showed negative inhomogeneity. With a temperature of 125 °C, films showed relatively better homogeneous behavior. This effect is depicted in Fig. 1. It is at this optimum temperature condition that we varied the oxygen pressure to study additional changes in the optical properties.

There is an additional interesting result regarding extinction coefficients in these films. It can be concluded from Fig. 5 that the mean extinction coefficients showed minimum values for the films deposited at ambient temperature. Bandgap analysis in the case of pure $ZrO_2$ shows very interesting results. A reported analysis on joint density states of various phases in $ZrO_2$ has revealed a double-peaked feature near the absorption edge, implying that there are more than one direct near-edge transitions.[42] Per our bandgap analysis, the composite films showed an indirect bandgap at 4.41 eV in addition to a direct gap at 4.62 eV, as shown in Fig. 6. A previous band-structure calculation on $\alpha$-$ZrO_2$ predicts an indirect gap at 4.51 eV close to one of our experimental values of 4.41 eV.[42] This implies that there is a small amount of monoclinic phase present in that deposition condition. This aspect is subsequently confirmed by x-ray diffraction analysis.

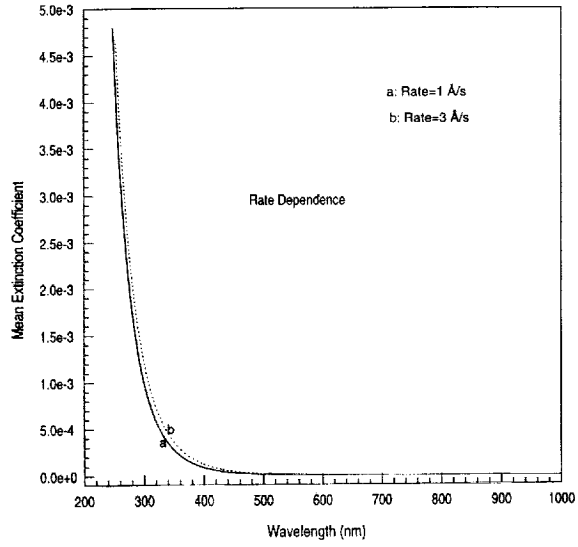


Fig. 12. Extinction coefficients of films deposited under different rates of evaporation but at the same oxygen pressure (base value) and substrate temperature (125 °C).

## 8. Effect of Oxygen Pressure

For oxide films, the oxygen pressure during the growth process controls the stoichiometry of the structure. The influence of oxygen concentration on optical properties of semi-insulating polycrystalline silicon films has been studied by Kucírková *et al.*[45] They observed a very pronounced effect of oxygen content on optical constants of the films. During our current experiments, oxygen pressure also showed the most dominant effect on the optical constants. The highest refractive indices were obtained at a pressure of $1 \times 10^{-4}$ mbar as shown in the Fig. 7. As the pressure during deposition was increased, however, the indices rapidly decreased. When the pressure was increased to $8 \times 10^{-4}$ mbar, the film indices decreased to a value as low as the substrate indices if observed inside the vacuum. When such films were

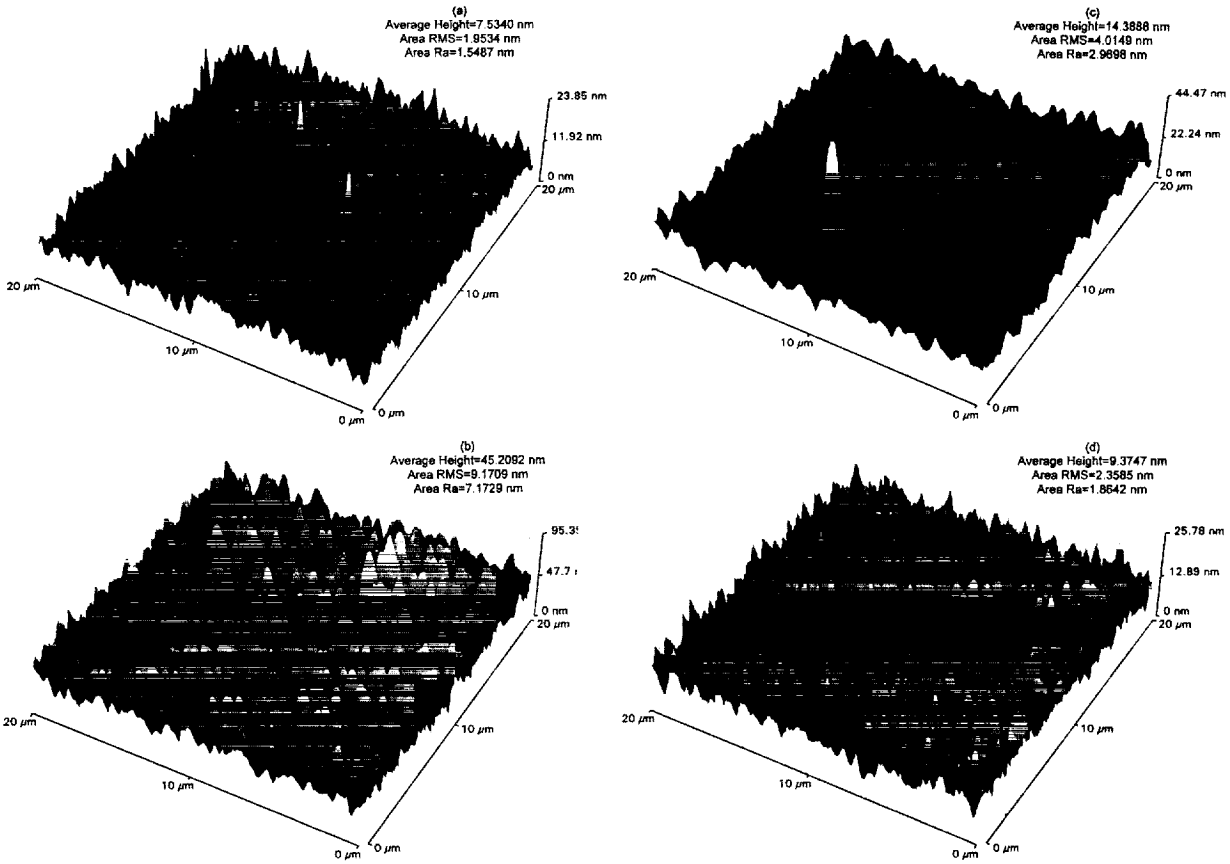


Fig. 14. (a) Surface topography of the film deposited at an optimum oxygen pressure of $1 \times 10^{-4}$ mbar, substrate temperature of 125 °C, and rate of 1 Å/s. The surface roughness has an area rms value of 1.9534 nm and a $R_a$ value of 1.5487 nm. (b) Surface topography of the film deposited at a higher oxygen pressure of $8 \times 10^{-4}$ mbar, substrate temperature of 125 °C, and rate of 1 Å/s. The surface roughness has an area rms value of 9.1709 nm and a $R_a$ value of 7.1729 nm. (c) Surface topography of the film deposited at the ambient temperature, oxygen base pressure and rate of 1 Å/s. The surface roughness has an area rms value of 4.0149 nm and a $R_a$ value of 2.9698 nm. (d) Surface topography of the film deposited at the highest experimental temperature of 239 °C and a oxygen base pressure and rate of 1 Å/s. The surface roughness has an area rms value of 2.3585 nm and a $R_a$ value of 1.8642 nm.

exposed to air, a large change in the index, indicative of a low packing density in the films, was observed. The vacuum-to-air transition of refractive index has been presented in the Fig. 8(a). It is also observed that such a transition can be minimized by sealing this portion of the layer with the subsequent deposition of a layer without any additional oxygen (i.e., higher packing density) and this leads to a more stable characteristic in air. This aspect was demonstrated by the successful development of a steep-edge filter. The sharp variation of refractive indices of the composite films over the higher end of the oxygen pressure scale tested gave us the idea of modulation.

Effects of oxygen pressure on pure $ZrO_2$ films have been investigated by several experimentalists.[40,46–52] It has been observed that these films are inherently rich with oxygen. When such films are deposited in an oxygen atmosphere, the excess oxygen embedded in the films yields superstoichiometric $ZrO_{2+x}$. Observations of these structures, primarily based on analysis of x-ray photoelectron spectroscopy, are reported by Khawaja *et al.*[47] They attributed this to be the cause of the lower refractive index at higher oxygen pressure. Similar experiments on MgO have generated a wide variety of results, with reports of films containing an excess of oxygen of as much as 40%. The presence of excess oxygen in these films also generates a superstoichiometric $MgO_x$ ($x > 1$) composition with high dielectric strength.[44,53] Likewise, in our experimental $ZrO_2$MgO composite films,

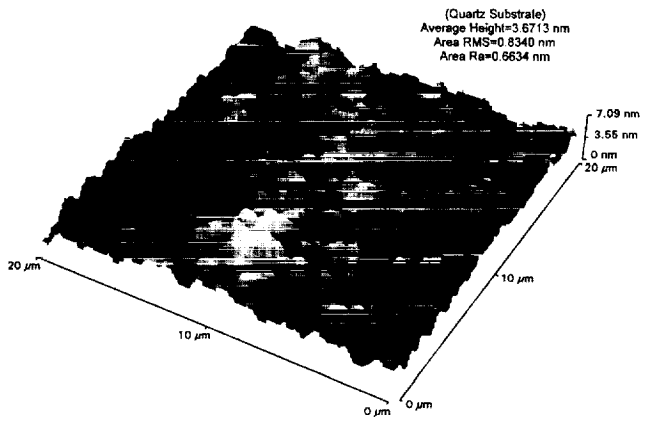


Fig. 15. Surface topography of the uncoated quartz substrate with the roughness having an area rms value of 0.8340 nm and a $R_a$ value of 0.6634 nm.

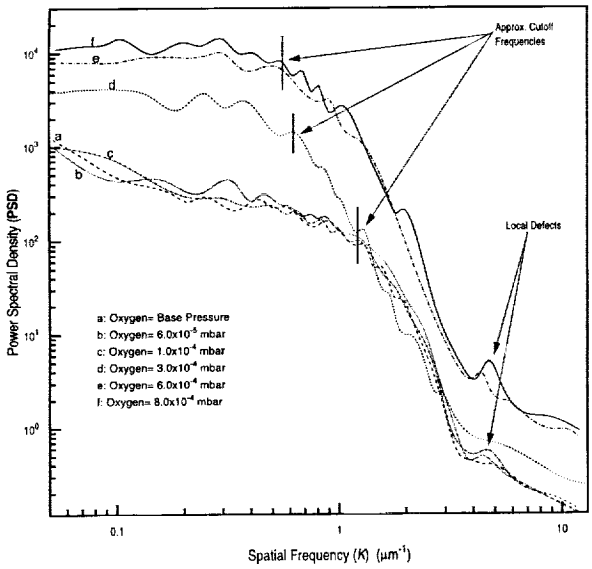


Fig. 16. Plot of the PSD versus spatial frequency for the films deposited under various oxygen pressures but at the same substrate temperature of 125 °C and rate of 1 Å/s.

the affinity for the oxygen has generated the interesting effect of causing a reduction of the mean refractive index down to a substrate value. These films showed highly negative inhomogeneity during their growth. Typical transmittance spectra taken just after the growth of the film in vacuum and then in air are presented in Fig. 8(b). It is clear that in air, the formerly highly inhomogeneous film becomes completely homogeneous with a sharp increase in the refractive index. This implies a poor packing density in the film.

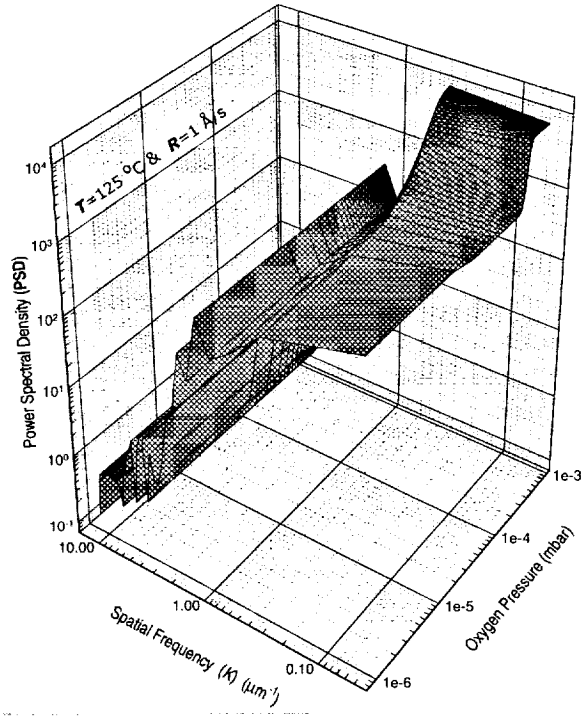


Fig. 17. Three-dimensional view of the PSD plots with respect to oxygen pressure, while substrate temperature (125 °C) and rate of deposition (1 Å/s) are constant.

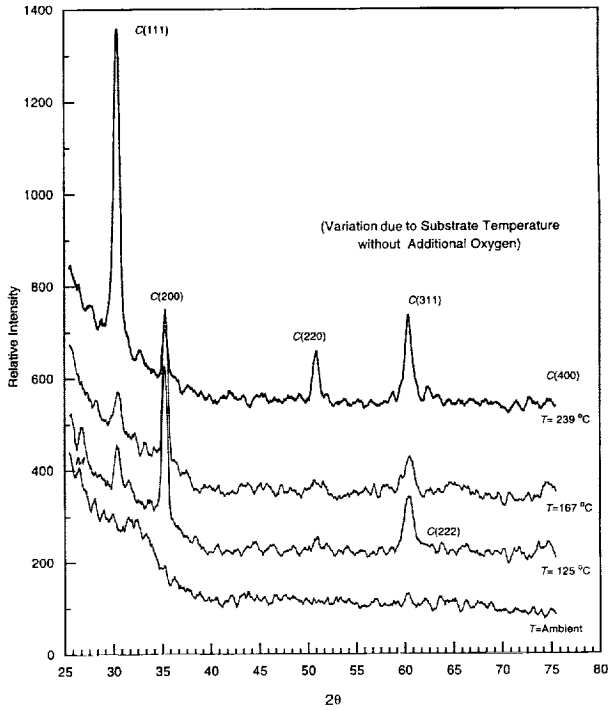


Fig. 18. X-ray diffraction peaks of the films deposited under different substrate temperatures but under the same rate of evaporation (1 Å/s) and the same oxygen base pressure.

The mean extinction coefficients showed an identical trend with respect to oxygen pressure. Samples prepared at $1 \times 10^{-4}$ mbar displayed the minimum optical losses as shown in Fig. 9, and samples prepared at $6 \times 10^{-4}$ mbar displayed the highest extinction coefficients. Similarly, as shown in Fig. 10, the

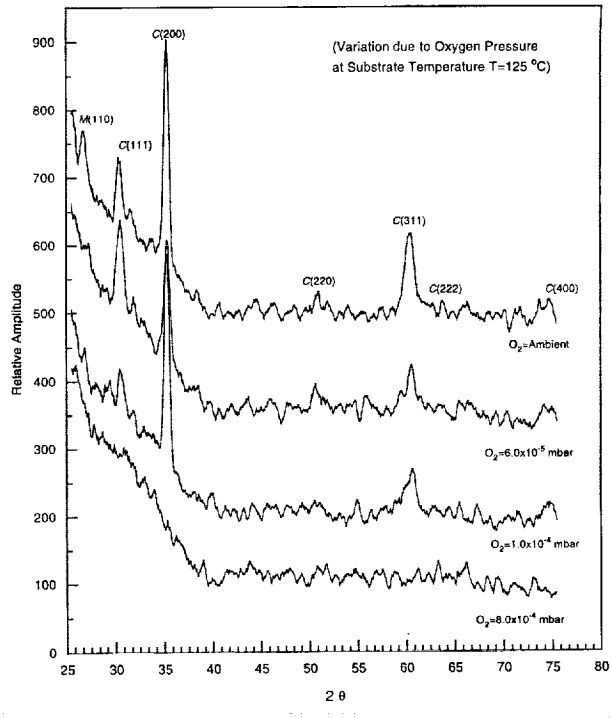


Fig. 19. X-ray diffraction peaks of the films deposited under different oxygen pressures but under the same rate of evaporation (1 Å/s) and the same substrate temperature.

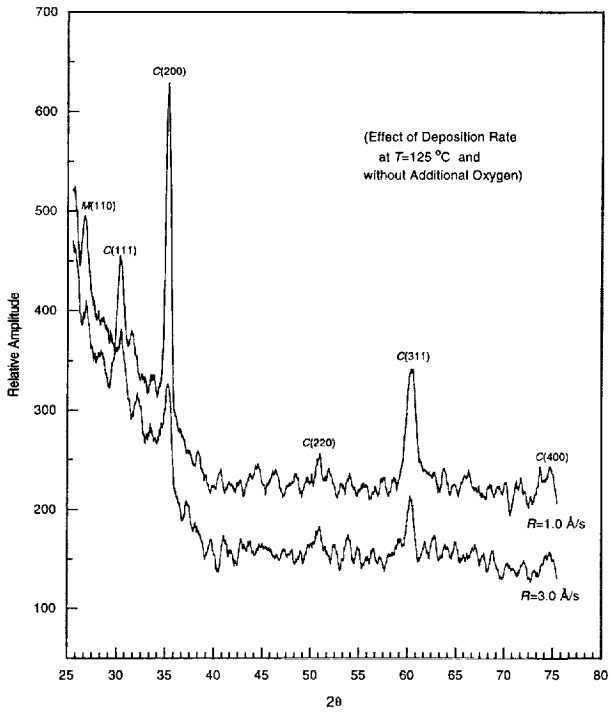


Fig. 20. X-ray diffraction peaks of the films deposited under different rates of evaporation but under the same substrate temperature and the same oxygen base pressure.

highest bandgap of 4.82 ev was obtained with samples prepared at the optimum values.

### 9. Effect of Rate of Evaporation

The rate of evaporation somewhat affected the films constants. Films prepared at a higher rate of evaporation showed relatively lower refractive index and higher extinction coefficients, as shown in Figs. 11 and 12. It is likely that the slower rate allows for a better stabilization of the nucleation process through a higher relaxation time, which, in turn, gives rise to a higher packing density and improved indices.[29] The most interesting effect observed in high-rate deposited films is the very prominent transition from homogeneous to inhomogeneous structures. Such a change was clearly observed during the *in situ* optical monitoring. The peak minima in the posttransmittance spectra also showed very different modulation behavior, as shown in Fig. 2. This effect was simulated assuming the presence of both homogeneous and inhomogeneous structures in the films along the growth direction, as depicted in Fig. 3.

### 10. Atomic Force Microscope Analysis

We used AFM for both qualitative as well as quantitative investigation of process-dependent properties. In these analyses, the morphological features, together with the roughness, can be acquired simultaneously over a wide range of spatial frequencies.[54–60] The equipment used for this portion of our investigation consisted of a Topometrix TMX 2000 series atomic force microscope. The probes used for the

**Table 2. Positions of 2θ Peaks for Our 15-Quarter-Wave-Thick Oxygen-Modulated Cubic Film along with Experimental and Theoretical Data[a]**

| | 2θ in 'Degrees' | | |
|---|---|---|---|
| ⟨hkl⟩ | (Present Work, 15 λ/4 $O_2$ Modulated Film) | (Reported by Duwez and Odell)[a] | (Theoretical)[a] |
| 111 | 30.52 | 30.57 | 30.50 |
| 200 | 35.36 | 35.43 | 35.35 |
| 220 | 50.87 | 50.66 | 50.86 |
| 311 | 60.52 | 60.44 | 60.48 |
| 222 | 63.49 | 63.47 | 63.46 |
| 400 | 74.74 | 74.85 | 74.84 |

[a]Ref. 61.

scans are standard $Si_3N_4$ pyramidal tips (1:1 aspect ratio, 4 μm × 4 μm) with triangular levers and 0.032-N/m spring constants.

For evaluating surface roughness, the current standard procedure is to use the PSD for topography description.[57] The statistical PSD function is defined as the square magnitude of the Fourier transform of the surface profile; it provides pertinent information concerning the amplitude of the surface features as a function of lateral spatial frequency.[55] Even for high-quality samples, a few localized defects (~1-μm radius) may still be present on the surface and produce a nonrandom spectrum.[54] Although these defects may be rather far (~50 μm) from one another, by coincidence the atomic force microscope tip may get positioned near one or more such defects, resulting a nonrandom spectrum. It is essential to point out that, in the presence of local defects, the nonrandom roughness can be predominant and alter all AFM analysis of random roughness.[54] In such cases, the use of analysis software is absolutely necessary to eliminate such points before determining the random roughness.

For uncoated quartz surfaces, the roughness spectrum follows approximately a straight line over several frequency decades on the log–log plot displayed in Fig. 13. This quasi-linear behavior of the PSD on a log–log scale is characteristic of a frequency variation given by[54]

$$\gamma(\sigma) = \phi/\sigma^{\psi}, \tag{12}$$

where $\phi$ is a constant, $\sigma$ is the spatial frequency, and $\psi$ is the spectrum slope. Depending on whether the parameter $\psi$ is greater or lower than 2, the surface may appear rougher or smoother as the wavelength increases.[56] For typical smooth surfaces this value is very close to 2. Such a power law may be characteristic of a fractal behavior of roughness or more specifically self-affine behavior.[54] In this situation we calculate expression of the two-dimensional fractal dimension $D$ as a function of spectrum slope[54]:

$$D = (8 - \psi)/2 = [(4\rho - \psi)/2], \tag{13}$$

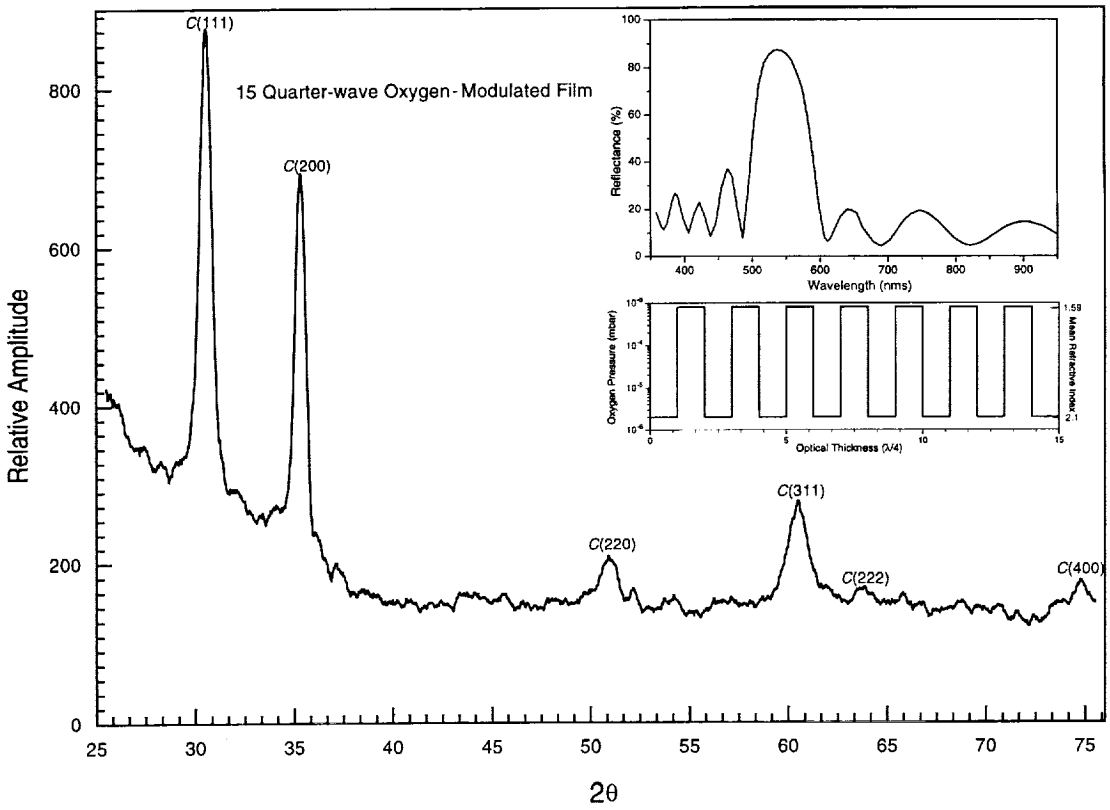


Fig. 21. X-ray diffraction peaks of a 15-quarter-wave oxygen-modulated film. The inset plots show oxygen pressure variation with respect to the physical thickness and the measured reflectance spectrum of the coating.

where ρ is the dimensional parameter. The parameter $D$ is quite informative in the case of AFM analysis; it describes how the roughness fills the space. The smoother the surface, the higher its $D$ value. We obtained a value of 2.85 ($\psi = 2.3$) for our bare quartz substrates, which means that our starting surface is reasonably smooth for the film deposition.

Surface topography of films deposited with oxygen pressure of 1 and $8 \times 10^{-4}$ mbars are presented in Figs. 14(a) and 14(b), respectively. As can be seen from these figures, the roughness and grain size of the films show maximum values for the films deposited at high oxygen pressure (average roughness, 45.21 nm). Films deposited at the optimum oxygen pressure of $1 \times 10^{-4}$ mbar showed a minimum average roughness of 7.53 nm. Deposition temperature alterations also produced very interesting changes in the surface topography. As can be seen from Figs. 14(c) and 14(d), films prepared at the maximum experimental temperature of 239 °C showed a quite smooth surface (9.37 nm) with more packed grains in comparison with the films prepared in ambient conditions (14.38 nm). In Fig. 15, the surface morphology of quartz substrate is depicted, which shows an average rms value of 0.834 nm over 20 μm × 20 μm scan size.

It is also possible to obtain information on relative grain size from the cutoff frequencies of the PSD.[55] In the case of PSD curves for thin-film samples, the spectral slope changes quite predominantly from a low to a high value and this point is designated as the cutoff frequency for the corresponding sample. It has already been established by Deumié *et al.*[54] that, in the case of thin-film samples, the variation in cutoff frequency is inversely proportional to the crystallite or grain size.[54] We also observed an identical trend in our samples. The samples deposited under high oxygen pressure showed larger grain size, which also can be observed in the PSD plots as shown in Fig. 16. The presence of additional small peaks at

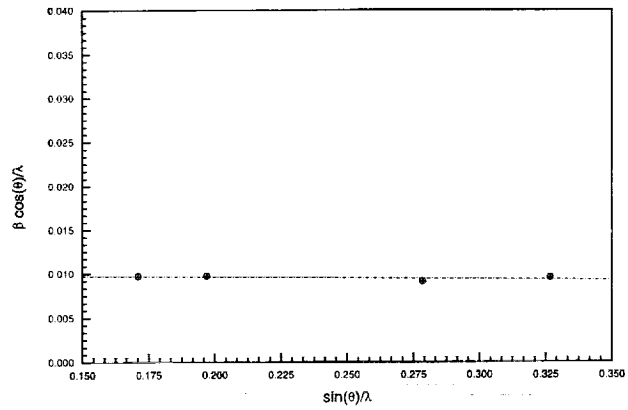


Fig. 22. Plot of β cos(θ)/λ versus sin(θ)/λ, which yields a linear plot parallel to the $x$ axis. This is indicative of a strain-free coating produced under oxygen modulation.

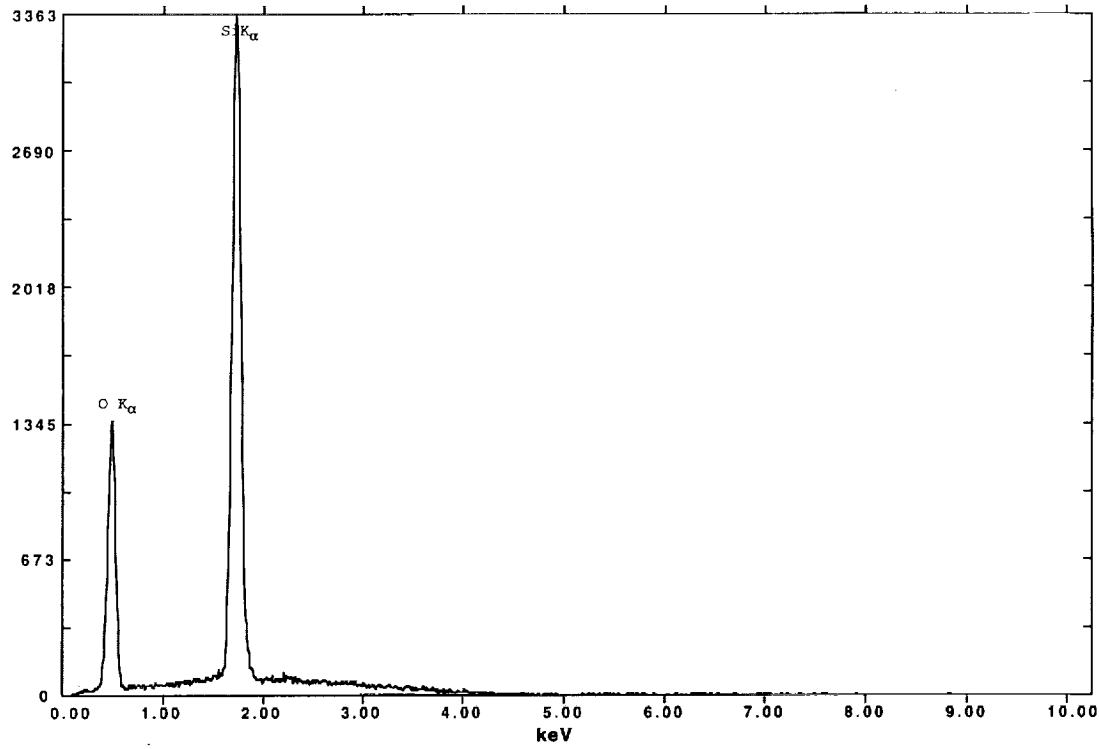


Fig. 23. EDX analysis of the uncoated quartz substrate.

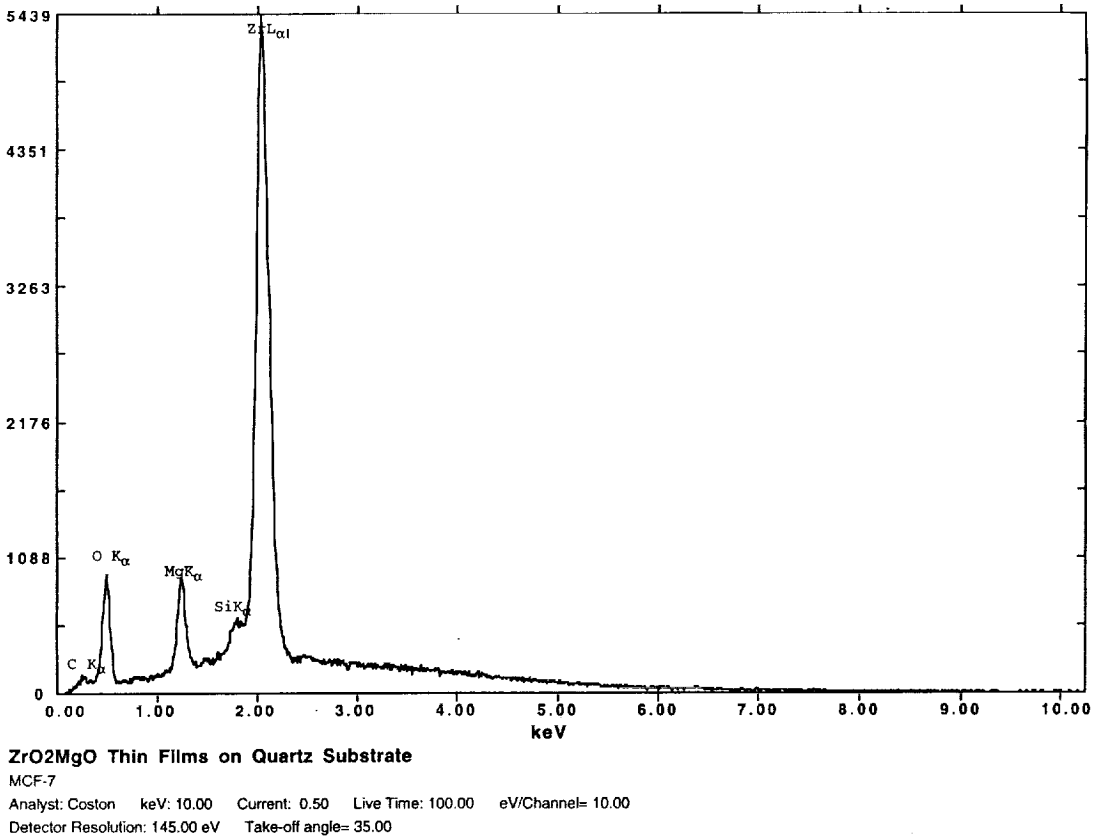


Fig. 24. EDX analysis of the film deposited under ambient substrate temperature and at a rate of 1 Å/s and oxygen base pressure. The relative peak heights for Zr:Mg:O are 1:0.175:0.178.

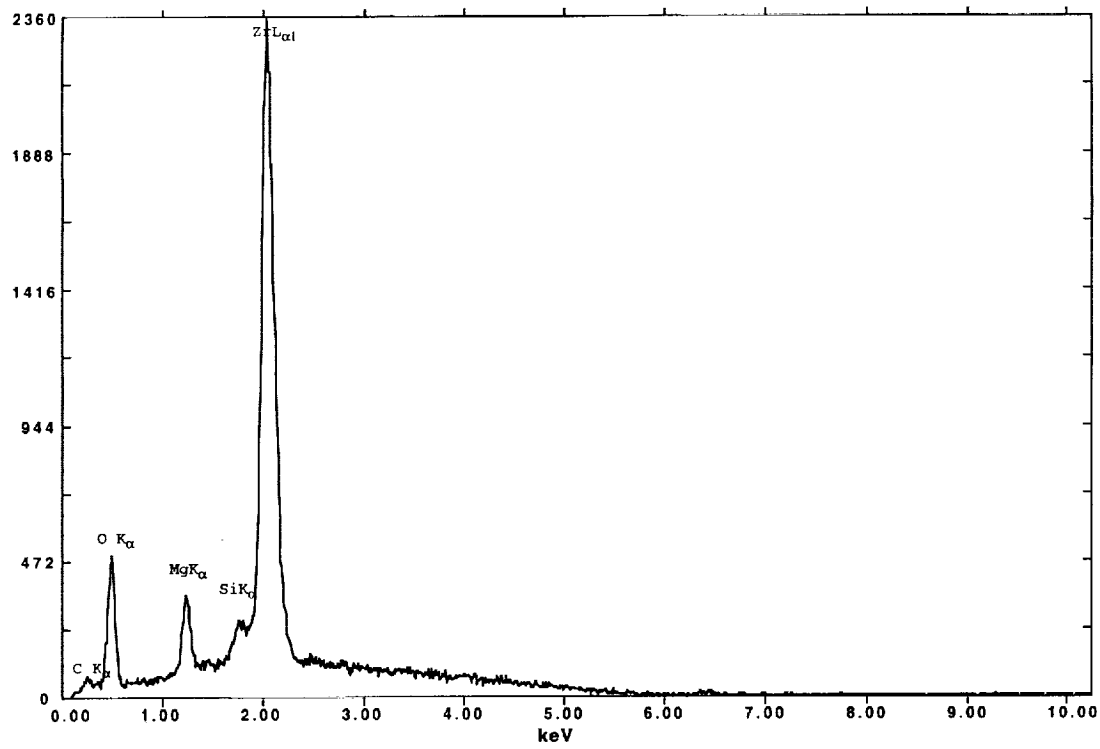


Fig. 25. EDX analysis of the film deposited at a substrate temperature of 167 °C and at a rate of 1 Å/s and base oxygen pressure. The relative peak heights for Zr:Mg:O are 1:0.152:0.211.

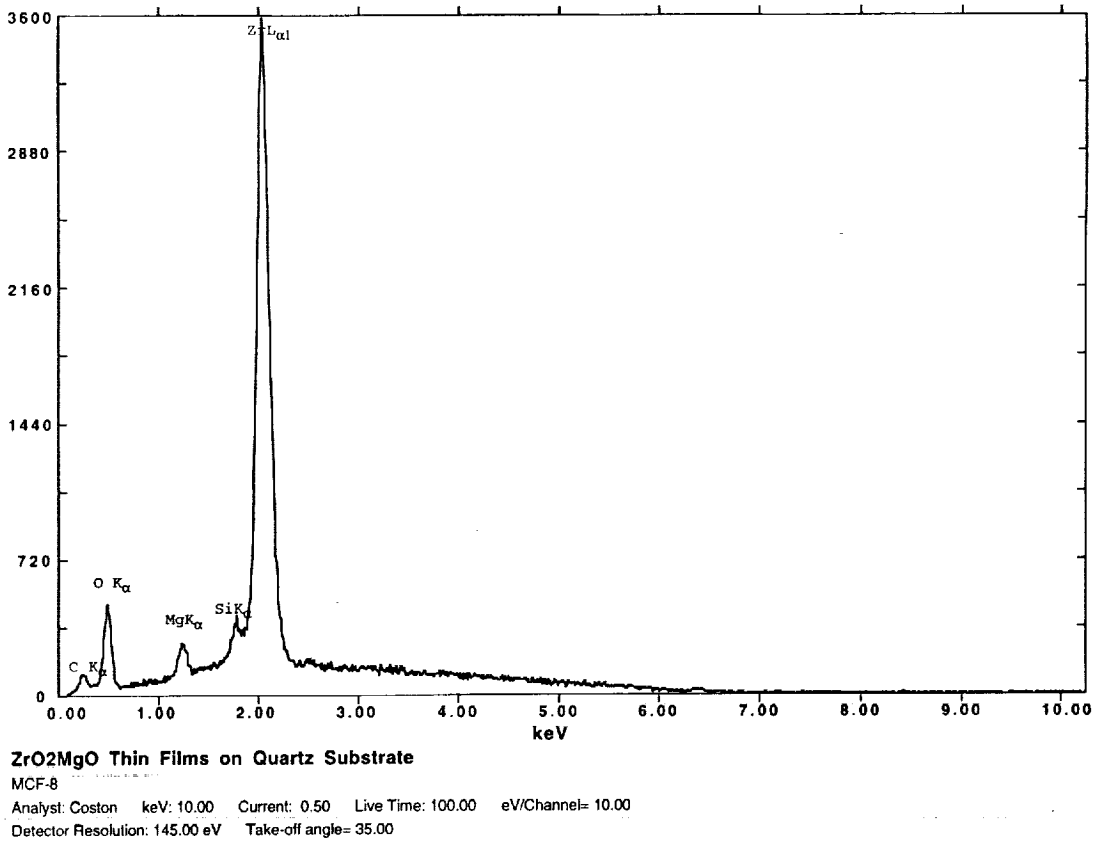


Fig. 26. EDX analysis of the film deposited under the highest experimental substrate temperature of 239 °C and at a rate of 1 Å/s and base oxygen pressure. The relative peak heights for Zr:Mg:O are 1:0.081:0.135.

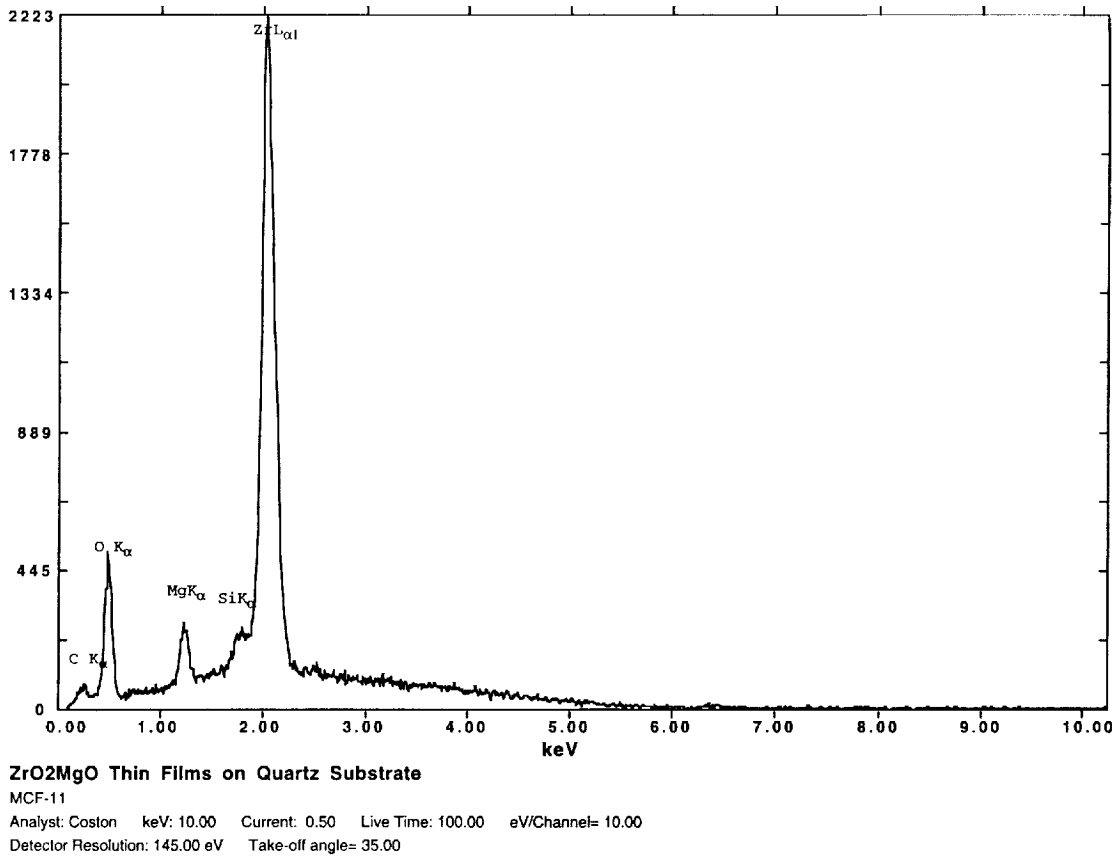


Fig. 27. EDX analysis of the film deposited at an oxygen pressure of $1 \times 10^{-4}$ mbar and at a rate of 1 Å/s and a substrate temperature of 125 °C. The relative peak heights for Zr:Mg:O are 1:0.127:0.228.

higher spatial frequency in these plots is indicative of local defects. It can be seen from these characteristics that the prevalence of such defects is a minimum for the films deposited at base oxygen pressure. In Fig. 17, we have presented the data in a three-dimensional form that clearly shows the sharp changes in the surface as a function of oxygen pressure in the high-pressure region. The decrease in the refractive indices at higher oxygen pressure can be attributed to a lowering of the packing density in the deposited films.

Atomic force microscope images also provided some qualitative information on the inhomogeneity in films. The samples with negative inhomogeneity (refractive indices decrease from the substrate–to–air interfaces) showed growth of crystallites that are more conical. This is evidence that these films are more densely packed and have a higher index of refraction near the substrate interface. The coated samples that were characterized as having negative inhomogeneity have optical transmission values at the half-wave turning points that exceed that of the bare substrates. The negative inhomogeneity in the films effectively produces a wide-band antireflection effect.

**Table 3. Relative SEM Peak Height Ratios of Zr:Mg:O for Various Sample Films Deposited under Different Process Conditions**

| Sub. Temp in °C | $O_2$ Pressure in mbar | Rate of Evap. Å/s | Zr:Mg:O (Relative Ratio) |
|---|---|---|---|
| Ambient | No Additional $O_2$ | 1.0 | 1:0.175:0.178 |
| 239 | No Additional $O_2$ | 1.0 | 1:0.081:0.135 |
| 167 | No Additional $O_2$ | 1.0 | 1:0.152:0.211 |
| 125 | $1.0 \times 10^{-4}$ | 1.0 | 1:0.127:0.228 |
| 125 | $8.0 \times 10^{-4}$ | 1.0 | 1:0.106:0.310 |

### 11. X-ray Diffraction Analysis

X-ray diffraction analysis of the samples grown with varied deposition parameters reveals very interesting differences in crystallographic phase and orientations of observed polycrystalloids. The diffraction spectra were recorded on a Rigaku (USA) diffractometer with Cu($K_\alpha$) ($\lambda$ = 1.5418 Å) radiation. The angular resolution for each sample was 0.02°. Since the films were deposited on quartz, the short-range order of $SiO_2$ contributes to the background structure, especially in the lower 2$\theta$ region.

Substrate temperature and oxygen pressure induced more significant changes compared with the rate of deposition. Except in the case in which coatings were deposited at ambient temperature, the cubic-phase peak was dominant, but the crystallographic orientation varied as deposition parameters were changed. The 2$\theta$ positions of the cubic-phase

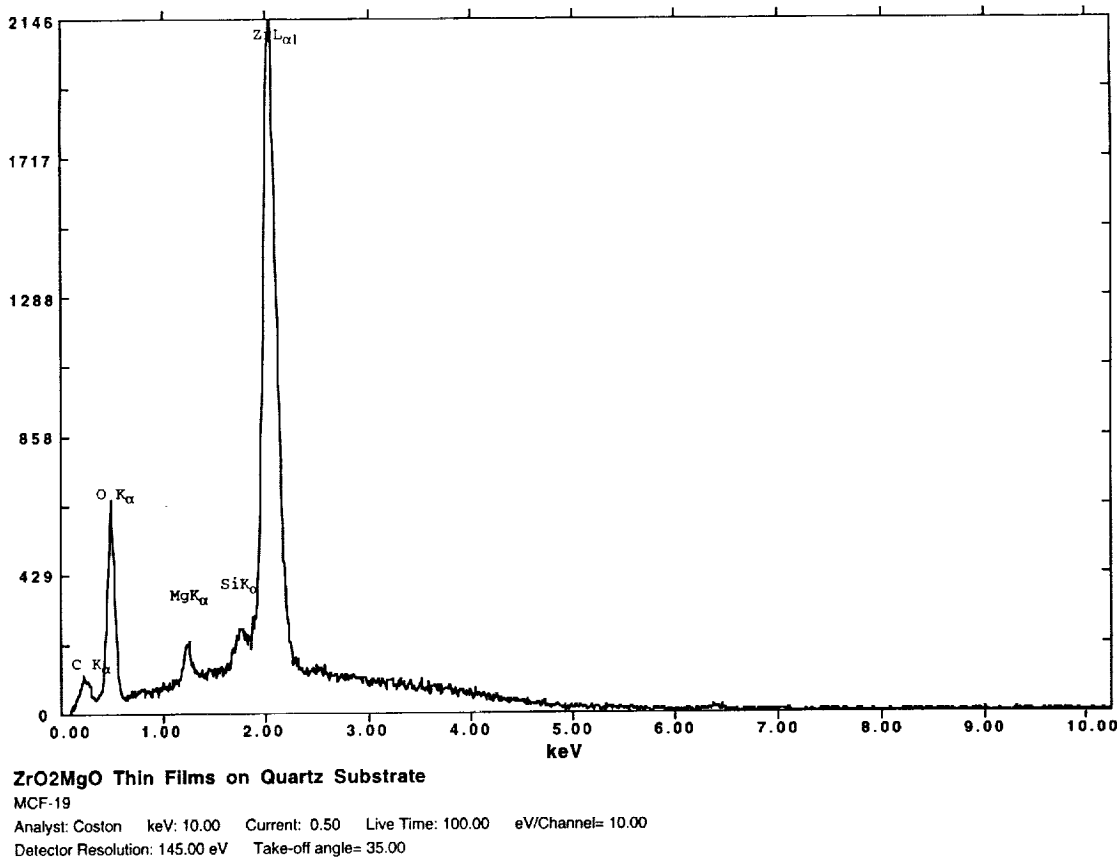


Fig. 28. EDX analysis of the film deposited at our highest experimental oxygen pressure of $8 \times 10^{-4}$ mbar and at a rate of 1 Å/s and a substrate temperature of 125 °C. The relative peak heights for Zr:Mg:O are 1:0.106:0.310.

peaks very well matched those reported by Duwez and Odell[61] for magnesia-stabilized cubic-zirconia samples. Samples prepared in ambient temperature conditions showed the presence of a very weak cubic phase in the films along with a trace of monoclinic phase as shown in Fig. 18. At a temperature of 239 °C, the film shows a very distinct cubic structure with the most preferred orientation being the ⟨111⟩ direction. For intermediate temperatures (167 °C and 125 °C), the most preferred orientation for crystalloids changed to the ⟨200⟩ direction. Note that in these phase conditions, the films had higher mean refractive indices and less inhomogeneity.

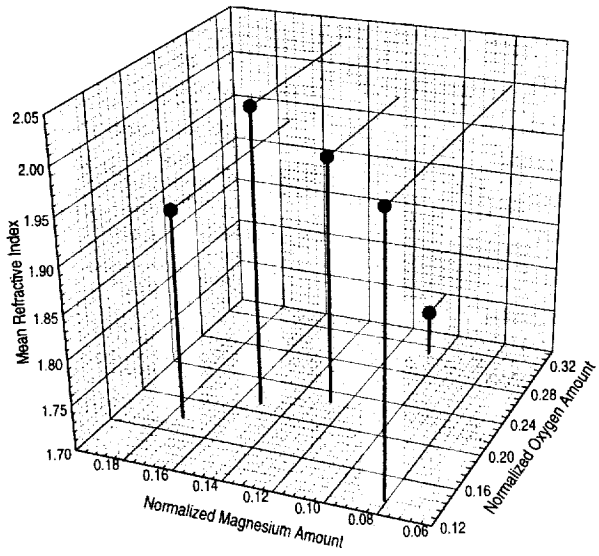


Fig. 29. Variation of mean refractive index with respect to both magnesium and oxygen contents.

Since the films showed minimum inhomogeneity at a substrate temperature of 125 °C, we attempted to minimize the inhomogeneity further by varying the oxygen pressure. Regardless of the oxygen pressure used, the films grew with the ⟨200⟩ direction being the most preferred orientation, as shown in Fig. 19. For films grown at a oxygen pressure of $8 \times 10^{-4}$ mbar, the crystallographic peaks were essentially absent, implying extreme randomness in the orientations of the crystallites. This is the condition that gave the lowest possible refractive indices of the films. Changes in the rate of evaporation also caused very distinct variations in the amplitudes of diffraction peaks, and this was most likely due to differences in the size and the orientation of the crystalloids. In Fig. 20, a comparison of peak amplitudes for films evaporated at rates of 1 Å and 3 Å/s are displayed.

Oxygen-pressure-modulated films showed the presence of the cubic structure very prominently. For example, Table 2 reports the position of the cubic

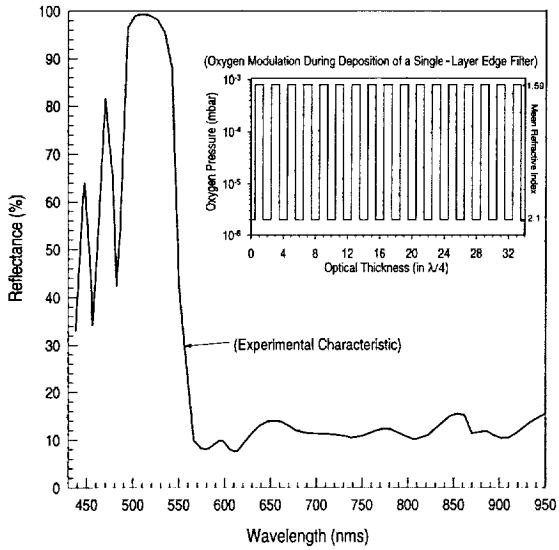


Fig. 30. Measured transmittance characteristic of a single-layer edge filter produced by oxygen modulation over an optical thickness of 34 quarter waves. The inset plot shows the oxygen modulation versus the optical thickness of the layer.

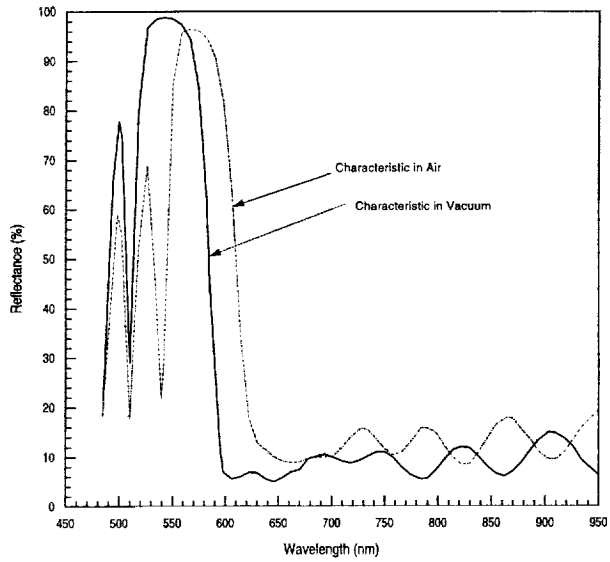


Fig. 31. Observed vacuum-to-air shift in the transmittance characteristics of an experimental edge filter.

peaks for 15-quarter-wave, oxygen-modulated film along with the reported peaks for the magnesia-stabilized (13.8 mol. %) $ZrO_2$ (cubic) peaks.[61] Figure 21 shows the diffraction pattern of this film in addition to the measured spectral reflectance and oxygen modulation along the growth direction.

For this modulated sample, we tried to find the effective residual strain and particle size from the x-ray peak broadening. Two major contributions for the peak broadening, effective particle size and strain, can be expressed in the following equations (for the isotropic case)[5,62,63]:

$$\beta/\lambda = 1/[P\cos(\theta)] + 4\varepsilon\tan(\theta)/\lambda, \quad (14)$$

$$\beta\cos(\theta)/\lambda = 1/P + 4\varepsilon\sin(\theta)/\lambda, \quad (15)$$

where $\beta$ is the full width at half-maximum (FWHM) of the Bragg peaks in radians, $\theta$ is the Bragg angle, $P$ is the effective coherent diffraction center size, $\varepsilon$ is the effective strain, and $\lambda$ is the wavelength of the x-rays. For distorted or anisotropic lattices, the equation becomes more complex. The fact that stress-induced diffraction peak broadening follows a $\tan(\theta)$ function, whereas the diffraction center size broadening has a $1/\cos(\theta)$ dependence, allows us to separate these effects graphically. From the above relationship, the diffraction center size and the strain are obtained when $\beta\cos(\theta)/\lambda$ versus $\sin(\theta)/\lambda$, which is depicted in the Fig. 22, is plotted. The value of $P$ computed from the intercept is ~10 Å. The slope of this plot is nearly zero, which suggests that such a film is almost strain-free.

Films deposited at two different rates of evaporation showed very distinct changes in x-ray diffraction peak heights and widths, as shown in Fig. 20. At the higher rate, the peaks are smaller, which is indicative of additional stress present in the film. This may be due to the rapid nucleation process with minimum relaxation time that occurs during higher-rate evaporation. Alternatively, there are several other possible explanations for the microstress in polycrystalline films that include dislocations, vacancies, defects, shear planes, thermal expansions, and contractions.

### 12. Energy-Dispersive X-Ray Compositional Analysis

To determine the cause of large variation in the refractive index in films prepared under relatively high oxygen pressure, we tried to investigate the variation in composition among the samples. Other investigators have pointed out that the relative amount of MgO in $ZrO_2$ substantially affects the optical and the structural properties. To measure the relative amount of Zr and Mg in the samples, we performed relative compositional analysis using the EDX feature available in a Hitachi SEM, Model S-4000. The electron-beam energy used was 10 KeV with a detector resolution of 145 eV. The carbon peak at 0.25 KeV is the usual peak associated with hydrocarbon contamination nearly always present on samples introduced from the laboratory environments. In Fig. 23, the EDX analysis of the uncoated quartz substrate is presented.

The ratio of the peak heights for the elements Mg and Zr provided very interesting information regarding the composition. The zirconium-to-magnesium ratio changes in the films deposited in different conditions, even though they all are evaporated from the same bulk material (Figs. 24–28). The detailed relative compositional ratios of Zr, Mg, and $O_2$ in various process conditions are presented in Table 3. The samples prepared at the highest substrate temperature shows the minimum amount of Mg with 1:0.081:0.135 as the ratio of Zr:Mg:O. The sample prepared at the highest oxygen pressure showed a relatively higher oxygen peak height although magnesium

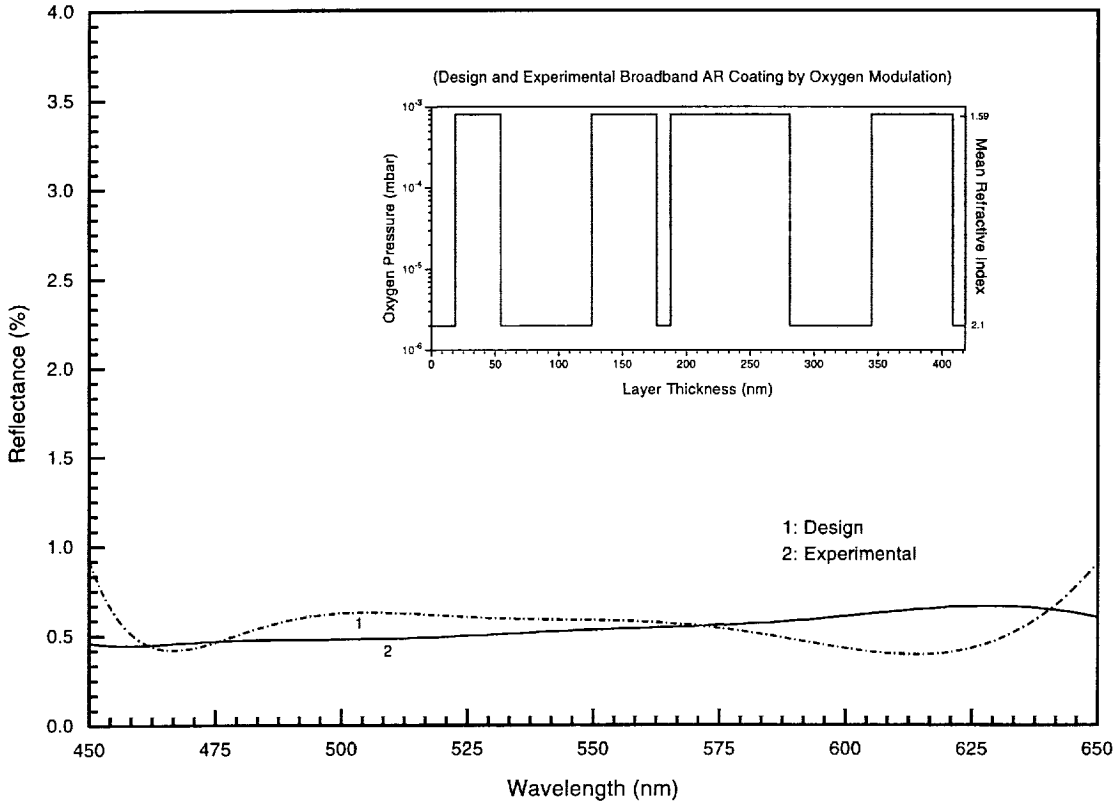


Fig. 32. Design and measured transmittance characteristics of a single-layer broadband antireflection coating produced by oxygen modulation. The inset plot shows the oxygen modulation with respect to the physical thickness of the layer.

peak was small. This can be attributed to the presence of water vapor in the film voids. The samples prepared at a temperature of 167 °C have the highest refractive index with a relative composition of 1:0.152 for Zr:Mg. In Fig. 29 we have plotted the mean refractive index with respect to both normalized magnesium and oxygen quantities. It can be seen from this plot that the highest mean refractive index, 2.023, has been obtained at an optimum magnesium (0.152) and oxygen (0.211) amount in the sample. This implies that an optimum level of MgO in the film produces a maximum value of the mean index. This observation is very interesting as a similar kind of compositional behavior has been reported by Tcheliebou *et al.*[16] for their coevaporated mixed $ZrO_2MgO$ films. Their study shows that it is possible to obtain the highest refractive index from mixed films that contain 15% mol of MgO, which is very much similar to our observation in the case of our solid solutions.

The possible explanation for the change in the ratio of zirconium to magnesium in samples prepared in different process conditions may be due to different nucleation and growth kinetics of the two constituent oxides ($ZrO_2$ and MgO) present in the solid solution. It is well known that refractory oxides, when deposited by electron-beam gun, first decompose and then recombine at the substrate. Since these two constituent oxides have different melting points, the corresponding accommodation coefficients ($a_c$), which is defined below, will be different.[64]

$$a_c = (t_i - t_e)/(t_i - t_s), \tag{16}$$

where $t_i$ is the temperature of the incident atoms, $t_e$ is the temperature of atoms reevaporating from the substrate, and $t_s$ is the temperature of the substrate. Similarly, the associated sticking coefficient and surface diffusion will be different for the two species depending on the oxygen pressure and the substrate temperature used during the deposition process, which effectively control the extent of oxidation as well as nucleation at the substrate surface. In our case, this probably led to a different ratio of zirconium and magnesium observed in different process conditions.

### 13. Results and Applications

The effects of various process parameters on optical properties were analyzed in depth. It was found that the refractive index strongly depends on both oxygen pressure and substrate temperature. The rate of evaporation has a relatively less dominant effect on optical properties. The substrate temperature controls the homogeneity of the films. At lower temperatures, the films were negatively inhomogeneous and at higher temperatures the films became positively homogeneous. The mean values for

refractive indices also changes with temperature, being highest at a value of 167 °C. At a temperature value of 125 °C, the films showed minimum inhomogeneity, although the mean refractive index was lower compared with the value at 167 °C. It is at this particular temperature that we varied the oxygen pressure. It was observed that the optical constants improved at a particular value of oxygen pressure. On both sides of this value, the constants deteriorated. The most significant change occurred when the pressure was below $2 \times 10^{-4}$ mbar. Here the index changes appreciably with the pressure. At oxygen pressure $6 \times 10^{-4}$ mbar, the films behave like medium index materials. At a value of $8 \times 10^{-4}$ mbar, however, the values almost matched the substrate values. This interesting change has enabled us to develop multilayer-equivalent-thin-film systems using the oxygen-modulated-single-film material. Unlike substrate temperature, oxygen pressure has the advantage in that it can be tuned quite rapidly during the deposition process. Hence one can achieve a continuously varied refractive in this material by suitably varying pressure during processing.

We have successfully developed various multilayer equivalent optical coatings using step modulation of oxygen during the growth of the film. In Fig. 21, we have presented the experimental characteristics of an oxygen-modulated 15-quarter-wave-thick film, which has a peak reflectance value of ~90% and a FWHM of 800 nm. The oxygen pressure modulation versus optical thickness of the film is also depicted below this plot. Similarly, using an optical thickness of 34 quarter waves in the film and suitably controlling the timings of modulation, we were able to generate characteristics of an edge filter equivalent to the design[65] 0.5H (LH) × 16 L 0.5H. The characteristics of such a single-layer coating is presented in Fig. 30. The oxygen pressure modulation versus layer thickness is also presented in this figure. Note from this experimental characteristic that the edge filter has a stop band over 495–545 nm and a passband with good ripple rejection starting from 565 nm. It carries a sharp transition in the reflectance that makes the coating an excellent wavelength multiplexer for use with closely spaced wavelengths. We have observed that, because of the change of refractive indices, there is a change of spectral characteristics measured in air and vacuum. In Fig. 31, we have presented the measured characteristics of an experimental edge filter in air and in vacuum. It can be observed from this plot that the characteristic in air has shifted to higher wavelengths with a decrease in reflectance over the stop band. This clearly indicates the increase of refractive index in the oxygen-enriched portion of the layer when exposed to air. In Fig. 32, we have shown the experimental characteristics of a more difficult antireflection coating. It has been observed in several modulated films that the vacuum-to-air shift in spectral characteristics becomes minimum when the last part of the film is deposited without any additional oxygen. Further experiments are in progress to minimize this effect.

## 14. Conclusion

We have investigated various process-dependent properties of the $ZrO_2MgO$ solid solution composite films deposited by reactive electron-beam evaporation. Substrate temperature and oxygen pressure affect the optical properties of the composite films in a very interesting manner. This is probably due to the formation of superstoichiometric structures in the films above a certain threshold value of oxygen pressure. SEM analysis has indicated the presence of a high ratio of oxygen in the films deposited at higher pressure. The optimum quantity of MgO in $ZrO_2$ needed to produce the highest refractive index is also determined by SEM measurements. The x-ray diffraction analysis showed various interesting results. Although most of the films showed cubic structure, the films deposited at ambient conditions reveal the presence of a small amount of monoclinic phase. This phase is also indicated by the indirect bandgap analysis. The refractive index reached its highest value for the films deposited at 167 °C without any additional oxygen. Films deposited at a temperature of 125 °C showed the highest refractive index when deposited at an oxygen pressure of $1 \times 10^{-4}$ mbar. At higher oxygen pressure, the films had refractive indices very similar to low-index film materials. Using suitable modulation of oxygen during the growth process made it possible to produce various types of optical coatings. The advantage of such coatings over their multilayer counterparts is the absence of discrete interfaces that are often the source of light-scattering defects. In addition, the standing-wave electric-field distribution of incident optical radiation does not encounter any discrete changes; this leads to higher damage threshold of such devices.

This research was performed while N. K. Sahoo held a National Research Council–NASA/Marshall Space Flight Center (MSFC) Research Associateship. The authors acknowledge the help of Marcus Vlasse of NASA/MSFC in carrying out the x-ray diffraction analysis and are also grateful to him for the useful technical discussions in interpreting the data. The authors thank J. E. Coston of NASA/MSFC for performing SEM analysis.

## References

1. J. A. Dobrowoloski and R. A. Kemp, "Refinement of optical multilayer systems with different optimization procedure," Appl. Opt. **29,** 2876–2893 (1990).
2. N. K. Sahoo and K. V. S. R. Apparao, "Modified complex method for constrained design and optimization of optical multilayer thin-film devices," Appl. Phys. A **59,** 317–326, (1994).
3. J.-S. Chen, S. Chao, J.-S. Kao, H. Niu, and C.-H. Chen, "Mixed films of $TiO_2$-$SiO_2$ deposited by double electron-beam coevaporation," Appl. Opt. **35,** 90–96 (1996).
4. H. Zhang and S. Liu, "Optical compound film deposited by double e-gun," Thin Solid Films **209,** 148–149 (1992).
5. S. B. Qadri, E. F. Skelton, P. Lubitz, N. V. Nguyen, and H. R.

Khan, "Electron beam deposition of $ZrO_2$-ZnO films," Thin Solid Films **290–291,** 80–83 (1996).
6. R. Bertram, M. F. Ouellette, and P. Y. Tse, "Inhomogeneous optical coatings: an experimental study of a new approach," Appl. Opt. **28,** 2935–2939 (1989).
7. W. J. Gunning, R. L. Hall, F. J. Woodberry, W. H. Southwell, and N. S. Gluck, "Codeposition of continuous composition rugate filters," Appl. Opt. **28,** 2945–2948 (1989).
8. R. Jacobsson, "Inhomogeneous and coevaporated homogeneous films for optical applications," Phys. Thin Films **8,** 51–98 (1975).
9. R. Jacobsson, "Optical properties of a class of inhomogeneous thin films," Opt. Acta **10,** 309–323 (1963).
10. A. Feldman, E. N. Farabaugh, W. K. Haller, D. M. Sanders, and R. A. Stempniak, "Modifying structure and properties of optical films by co-evaporation," J. Vac. Sci. Technol. A **4,** 2969–2974 (1986).
11. J. P. Cheron, F. Tcheliebou, and A. Boyer, "Structural properties of $Y_2O_3$ stabilized $ZrO_2$ films deposited by reactive thermal coevaporation," J. Vac. Sci. Technol. A **10,** 3207–3209 (1992).
12. M. Mesbah, A. Boyer, E. Groubert, and L. Martin, "Crystallographic and optical study of $ZrO_2$ partially and totally stabilized with $Y_2O_3$," J. Vac. Sci. Technol. A **8,** 3961–3966 (1990).
13. C. M. Gilmore, C. Quinn, S. B. Qadri, C. R. Gosset, and E. F. Skelton, "Stabilization of tetragonal $ZrO_2$ with $Al_2O_3$ in reactive magnetron sputtered thin films," J. Vac. Sci. Technol. A **5,** 2085–2087 (1987).
14. Y. Tsou and F. C. Ho, "Optical properties of hafnia and coevaporated hafnia magnesium fluoride thin films," Appl. Opt. **35,** 5091–5094 (1996).
15. S. B. Qadri, E. F. Skelton, M. Z. Harford, R. Jones, and P. Lubitz, "$e^-$-beam deposition of $In_2O_3$ stabilized $ZrO_2$ films," J. Vac. Sci Technol. A **9,** 510–511 (1991).
16. F. Tcheliebou, A. Boyer, and L. Martin, "Studies on MgO-stabilized zirconia thin films in the UV-visible region," Thin Solid Films **249,** 86–90 (1994).
17. D. M. Sanders, E. N. Farabaugh, and W. K. Haller, "Glassy optical coatings by multisource evaporation," in *Thin Film Technologies and Special Applications*, W. R. Hunter, ed., Proc. SPIE **346,** 31–38 (1982).
18. E. N. Farabaugh and D. M. Sanders, "Microstructure of dielectric thin films formed by e-beam coevaporation," J. Vac. Sci. Technol. A **1,** 356–359 (1983).
19. D. L. Porter and A. H. Heuer, "Microstructural development in MgO-stabilized zirconia (Mg-PSZ)," J. Am. Ceram. Soc. **62,** 298–305 (1979).
20. M. M. El-Nahass, B. A. Khalifa, A. M. Abd El-Rahman, and R. El-Ariny, "Structural and optical properties of $ZnSe_xTe_{1-x}$ solid solution in thin film form," Appl. Phys. A **63,** 81–86 (1996).
21. R. H. Hannink, "Microstructural development of sub-eutectoid aged MgO–$ZrO_2$ alloys," J. Mater. Sci **18,** 457–470 (1983).
22. M. J. Readey, A. H. Heuer, and R. W. Steinbrech, "Annealing of test specimens of high-toughness magnesia-partially-stabilized zirconia," J. Am. Ceram. Soc. **71,** c2–c6 (1988).
23. M. L. Balmer, F. F. Lange, and C. G. Levi, "Metastable phase selection and partitioning in $ZrO_2$-MgO processed from liquid precursors," J. Am. Ceram. Soc. **75,** 946–952 (1992).
24. C. F. Grain, "Phase relations in the $ZrO_2$-MgO system," J. Am. Ceram. Soc. **50,** 288–290 (1967).
25. N. H. Brett, M. Gonzalez, J. Bouillot, and J. C. Niepce, "Neutron and x-ray diffraction studies on pure and magnesia-doped zirconia gels decomposed in vacuo," J. Mater. Sci **19,** 1349–1358 (1984).
26. O. Ruff and F. Ebert, "Ceramics of highly refractory materials," Z. Anorg. Allgem. Chem. **180,** 19–41 (1929).
27. H. J. Rossel and R. H. J. Hannink, "The phase $Mg_2Zr_5O_{12}$ in MgO partially stabilized zirconia," in *Science and Technology of Zirconia II*, Vol. 12 of Advances in Ceramics, N. Claussen, M. Rühle, and A. H. Heuer, eds. (The American Ceramic Society, Inc., Columbus, Ohio, 1984), pp. 139–151.
28. D. L. Wood and K. Nassau, "Refractive index of cubic zirconia stabilized with yttria," Appl. Opt. **21,** 2978–2981 (1982).
29. N. K. Sahoo and K. V. S. R. Apparao, "Process-parameter optimization of $Sb_2O_3$ films in the ultraviolet and visible region for interferometric applications," Appl. Phys. A **63,** 195–202 (1996).
30. B. Bovard, F. J. Van Milligen, M. J. Messerly, S. G. Saxe, and H. A. Macleod, "Optical constants derivation for an inhomogeneous thin film from *in situ* transmission measurements," Appl. Opt. **24,** 1803–1807 (1985).
31. D. P. Arndt, R. M. A. Azzam, J. M. Bennett, J. P. Borgogno, C. K. Carniglia, W. E. Case, J. A. Dobrowolski, U. J. Gibson, T. Tuttle Hart, F. C. Ho, V. A. Hodgkin, W. P. Klapp, H. A. Macleod, E. Pelletier, M. K. Purvis, D. M. Quinn, D. H. Strome, R. Swenson, P. A. Temple, and T. F. Thonn, "Multiple determination of the constants of thin-film coating materials," Appl. Opt. **23,** 3571–3596 (1984).
32. M. Nowak, "Determination of optical constants and average thickness of inhomogeneous-rough thin films using spectral dependence of optical transmittance," Thin Solid Films **254,** 200–210 (1995).
33. J. P. Borgogno, B. Lazarides, and E. Pelletier, "Automatic determination of the optical constants of inhomogeneous thin films," Appl. Opt. **21,** 4020–4029 (1982).
34. E. E. Khawaja, "The determination of the refractive index and thickness of a transparent film," J. Phys. D. **9,** 1939–1943 (1976).
35. R. Swanepoel, "Determination of the thickness and optical constants of amorphous silicon," J. Phys. E **16,** 1214–1222 (1983).
36. J. P. Borgogno, P. Bousquet, F. Flory, B. Lazarides, E. Pelletier, and P. Roche, "Inhomogeneity in films: limitation of the accuracy of optical monitoring of thin films," Appl. Opt. **20,** 90–94 (1981).
37. M. Harris, H. A. Macleod, S. Ogura, E. Pelletier, and B. Vidal, "The relationship between optical inhomogeneity and film structure," Thin Solid Films **57,** 173–178 (1979).
38. S. Ogura, "Dynamic characteristics in optically inhomogeneous films," in *Thin Films for Optical Systems*, K. H. Guenther, ed., Proc. SPIE **1782,** 377–388 (1992).
39. G. Ghosh, "Sellmeier coefficients and dispersion of thermo-optic coefficients for some optical glasses," Appl. Opt. **36,** 1540–1546 (1997).
40. C.-K. Kwok and C. R. Aita, "The transition from $\alpha$Zr to $\alpha ZrO_2$ growth in sputter-deposited films as a function of gas $O_2$ content, rare-gas type and cathode voltage," J. Vac. Sci Technol. A **7,** 1235–1239 (1989).
41. C.-K. Kwok and C. R. Aita, "Near-bandgap optical behavior of sputter deposited $\alpha$- and $\alpha + \beta -$ $ZrO_2$ films," J. Appl. Phys. **66,** 2756–2758 (1989).
42. C.-K. Kwok and C. R. Aita, "Indirect band gap in $\alpha$-$ZrO_2$," J. Vac. Sci Technol. A **8,** 3345–3346 (1990).
43. A. V. Tikhonravov, M. K. Trubetskov, A. N. Tikhonov, O. B. Tcsherednichenko, B. G. Lysoi, K. V. Mikhailova, B. T. Sullivan, and J. A. Dobrowolski, "Study of thin film inhomogeneity with a fast-scanning acoustooptic spectrophotometer," in *Developments in Optical Component Coatings*, I. Reid, ed., Proc. SPIE **2776,** 212–220 (1996).
44. A. F. Hebard. A. T. Fiory, S. Nakahara, and R. H. Eick, "Oxygen-rich polycrystalline magnesium oxide—a high quality thin-film dielectric," Appl. Phys. Lett. **48,** 520–522 (1986).
45. A. Kucírková, K. Navrátil, L. Pajasová, and V. Vorlícek, "Influence of oxygen concentration on optical properties of semi-insulating polycrystalline silicon films," Appl. Phys. A **63,** 495–503 (1996).
46. F. Jones, "High-rate reactive sputter deposition of zirconium dioxide," J. Vac. Sci. Technol. A **6,** 3088–3097 (1988).
47. E. E. Khawaja, F. Bouamrane, A. B. Hallak, M. A. Daous, and

M. A. Salim, "Observation of oxygen enrichment in zirconium oxide films," J. Vac. Sci Technol. A **11,** 580–587 (1993).
48. M. Yoshitake, K. Takiguchi, Y. Suzuki, and S. Ogawa, "Effect of oxygen pressure in reactive ion-beam sputter deposition of zirconium oxides," J. Vac. Sci. Technol. A **6,** 2326–2332 (1988).
49. P. J. Martin, R. P. Netterfield, and W. G. Sainty, "Modification of the optical and structural properties of dielectric $ZrO_2$ films by ion-assisted deposition," J. Appl. Phys. **55,** 235–241 (1984).
50. H. J. Cho and C. K. Hwangbo, "Optical inhomogeneity and microstructure of $ZrO_2$ thin films prepared by ion-assisted deposition," Appl. Opt. **35,** 5545–5552 (1996).
51. R. E. Klinger and C. K. Carniglia, "Optical and crystalline inhomogeneity in evaporated zirconia films," Appl. Opt. **24,** 3184–3187 (1985).
52. J. A. Dobrowolski, P. D. Grant, R. Simpson, and A. J. Waldorf, "Investigation of the evaporation process conditions on the optical constants of zirconia films," Appl. Opt. **28,** 3997–4005 (1989).
53. P. Vuoristo, T. Mäntylä, P. Kettunen, and R. Lappalainen, "RBS analysis of sputter-deposited MgO films," Vacuum **42,** 1001–1004 (1991).
54. C. Deumié, R. Richier, P. Dumas, and C. Amra, "Multiscale roughness in optical multilayers: atomic force microscopy and light scattering," Appl. Opt. **35,** 5583–5594 (1996).
55. F. Biscarini, P. Samorí, A. Lauria, P. Ostoja, R. Zamboni, C. Taliani, P. Viville, R. Lazzaroni, and J. L. Brédas, "Morphology and roughness of high-vacuum sublimed oligomer thin films," Thin Solid Films **284-285,** 439–443 (1996).
56. C. Amra, C. Deumié, D. Torricini, P. Roche, R. Galindo, P. Dumas, and F. Salvan, "Overlapping of roughness spectra measured in macroscopic (optical) and microscopic (AFM) bandwidths," in *Optical Interference Coatings*, F. Abeles, ed., Proc. SPIE **2253,** 614–630 (1994).
57. A. Duparré and S. Jakobs, "Combination of surface characterization techniques for investigating optical thin-film components," Appl. Opt. **35,** 5052–5058 (1996).
58. T. K. S. Wong and W. K. Man, "Scanning probe microscopy and tunneling measurements of polycrystalline tin oxide films," Thin Solid Films **287,** 45–50 (1996).
59. I. Y. Sokolov, "On the recovery of the spectroscopic image in atomic force microscopy," J. Vac. Sci. Technol. A **14,** 2901–2904 (1996).
60. U. Kaiser, M. Adamik, G. Sáfrán, P. B. Barna, S. Laux, and W. Richter, "Growth structure investigation of $MgF_2$ and $NdF_3$ films grown by molecular beam deposition on $CaF_2$ (111) substrates," Thin Solid Films **280,** 5–15 (1996).
61. P. Duwez and F. Odell, "Phase relationships in the system zirconia-ceria," J. Am. Ceram. Soc. **33,** 274–283 (1950).
62. W. H. Hall, "X-ray line broadening in metals," Proc. Phys. Soc. London Sec. A **62,** 741–743 (1949).
63. R. Jenkins and R. L. Snyder, *Introduction to X-ray Powder Diffractometry* (Wiley-Interscience, New York, 1996).
64. B. Lewis and J. C. Anderson, *Nucleation and Growth of Thin Films* (Academic, New York, 1978).
65. H. A. Macleod, *Thin Film Optical Filters*, 2nd ed. (Macmillan, New York, 1986), Chap. 6, p. 194.